Inorganic Chemistry
Article

Inorg. Chem. **2010**, *49*, 8255–8269 **8255**
DOI: 10.1021/ic100413x

Heteropolynuclear Gold Complexes with Metallophilic Interactions: Modulation of the Luminescent Properties

Maria José Calhorda,[‡] Carmen Ceamanos,[†] Olga Crespo,[†] M. Concepción Gimeno,*[,†] Antonio Laguna,[†] Carmen Larraz,[†] Pedro D. Vaz,[‡] and M. Dolores Villacampa[†]

[†]*Departamento de Química Inorgánica, Instituto de Ciencia de Materiales de Aragón, Universidad de Zaragoza-C.S.I.C., E-50009 Zaragoza, Spain, and* [‡]*Departamento de Química e Bioquímica, CQB, Faculdade de Ciências da Universidade de Lisboa, Campo Grande, 1749-016 Lisboa, Portugal*

Received March 2, 2010

Metalloligands of stoichiometry [AuCl(P−N)] have been obtained by the reaction of the heterofunctional phosphines P−N = PPh_2py, $PPh_2CH_2CH_2py$, or $PPhpy_2$ with [AuCl(tht)] (tht = tetrahydrothiophene). Reactions of these metalloligands with several metal compounds have afforded heteropolynuclear species which exhibit luminescent properties. The stoichiometries depend on the molar ratio and the heterometal. Thus, the reaction with $[Cu(NCMe)_4]^+$ in a molar ratio 2:1 gives the trinuclear compounds $[Au_2CuCl_2(P-N)_2]^+$, in which the structure and Au···Cu interactions depend on the phosphine ligand. With rhodium and iridium derivatives the reactivity is different leading to complexes of the type $[AuMCl_2(cod)(P-N)]$ for P−N = PPh_2py, $PPhpy_2$, and $[Au_2M_2Cl(cod)_2(P-N)_2]Cl$ with $PPh_2CH_2CH_2py$. Using $[MCl_2(NCPh)_2]$ (M = Pd, Pt) in a 2:1 molar ratio yields $[Au_2MCl_4(P-N)_2]$ and in a 1:1 molar ratio $[AuPdCl_3(\mu_3\text{-}PPhpy_2)]$. Several compounds have been characterized by X-ray diffraction showing in many cases short Au···M distances. The luminescence of these derivatives has been studied. The metalloligands display bands assigned to intraligand (IL) transitions. For the bimetallic (Au/M) systems the luminescence depends on the heterometal present and on the metallophilic interactions. The most important excitations in the relevant energy range were assigned essentially a MMLCT character (from Rh/Ir and Au to ligands) based on density functional theory (DFT) calculations in selected complexes. The luminescence behavior in Rh/Ir $[AuMCl_2(cod)(PPh_2py)]$ complexes was interpreted on the basis of the different nature of the half occupied orbitals in the triplet state.

Introduction

The chemistry of gold has received much attention in the past years in view of the intriguing features presented by its complexes as, for example, the tendency of gold complexes to aggregate into oligomers or supramolecular assemblies through metal−metal interactions.[1,2] These secondary bonds often result in the interesting photochemical and photophysical properties of the gold-containing complexes. Indeed, it has been shown in many examples that their luminescence originates from these aurophilic interactions.[3,4] Heterometallic gold species are also receiving a great deal of attention because the interaction between gold atoms and other metal centers may give rise to unusual structural frameworks and properties, as exemplified in mixed complexes with several metals such as silver, copper, thallium, mercury, and so forth. Many of them present interesting luminescent properties that are enhanced by the presence of these metallophilic interactions. Such heterometallic complexes can be obtained by reaction of $[AuR_2]^-$ salts with metal centers which lead to donor−acceptor species,[5] by the reaction of trinuclear gold species $[Au_3(L\text{-}L)_3]$,[6] from the metallocryptands $[Au_2(L\text{-}L)_3]^{2+}$,[7] or by reaction of $[Au(CN)_2]^-$ salts with different metals.[8] However, the origin

*To whom correspondence should be addressed. E-mail: gimeno@unizar.es.

(1) (a) *Gold, Progress in Chemistry, Biochemistry and Technology*; Schmidbaur, H., Ed.; John Wiley & Sons: New York, 1999. (b) *Modern Supramolecular Gold Chemistry: Gold-Metal Interactions and Applications*; Laguna, A.; Ed. Wiley-VCH: New York, 2008.

(2) Gimeno, M. C.; Laguna, A. *Comprehensive Coordination Chemistry II*; McCleverty, J. A., Meyer, T. J., Eds.; Elsevier: New York, 2003; Vol. *5*, pp 911−1145.

(3) (a) Forward, J. M.; Fackler, J. P. Jr.; Assefa, Z. *Optoelectronic Properties of Inorganic Compounds*; Roundhill, D. M., Fackler, J. P. J., Eds.; Plenum Press: New York, 1999; pp 195−230. (b) Balch, A. L. *Gold Bull.* **2004**, *37*, 1–2. (c) Yam, V. W. W.; Chan, C. L.; Li, C. K.; Wong, K. M. C. *Coord. Chem. Rev.* **2001**, *216−217*, 173–194. (d) Yam, V. W. W. *Chem. Soc. Rev.* **2008**, *37*, 1806–1813.

(4) (a) Lee, Y. A.; Eisenberg, R. *J. Am. Chem. Soc.* **2003**, *125*, 7778–7779. (b) Mansour, M. A.; Connick, W. B.; Lachicotte, R. J.; Gysling, H. J.; Eisenberg, R. *J. Am. Chem. Soc.* **1998**, *120*, 1329–1320.

(5) (a) Fernández, E. J.; Gimeno, M. C.; Laguna, A.; López de Luzuriaga, J. M.; Monge, M.; Pyykkö, P.; Sundholm, D. *J. Am. Chem. Soc.* **2000**, *122*, 7287–7293. (b) Fernández, E. J.; López de Luzuriaga, J. M.; Monge, M.; Olmos, M. E.; Pérez, J.; Laguna, A.; Mohamed, A. A.; Fackler, J. P., Jr. *J. Am. Chem. Soc.* **2003**, *125*, 2022–2033.

(6) (a) Burini, A.; Fackler, J. P., Jr.; Galassi, R.; Pietroni, B. R.; Staples, R. J. *Chem. Commun.* **1998**, 95–96. (b) Burini, A.; Fackler, J. P., Jr.; Galassi, R.; Grant, T. A.; Omary, M. A.; Rawashdeh-Omary, M. A.; Pietroni, B. R.; Staples, R. J. *J. Am. Chem. Soc.* **2000**, *122*, 11264–11265.

(7) (a) Catalano, V. J.; Bennett, B. L.; Kar, H. M. *J. Am. Chem. Soc.* **1999**, *121*, 10235–10236. (b) Catalano, V. J.; Malwitz, M. A. *J. Am. Chem. Soc.* **2004**, *126*, 6560–6561.

Published on Web 08/19/2010

of the luminescent properties may be associated with such different factors as the nature of the ligand and the heterometal, or the presence or absence of metalophilic interactions. Not many systematic studies of the luminescence properties of heterometallic entities with different ligands and metals have been published. We have previously reported the reaction of chalcogenide gold complexes of stoichiometry $[E\{Au(P-N)\}_3]^+$, where P−N represents a heterofunctional ligand with silver or copper derivatives, which led to highly luminescent derivatives.[9] However, the study could not be extended to many metal centers owing to the specific coordination requirements of the metalloligands. Therefore, in this work our aim was to synthesize heteropolynuclear derivatives of gold with potential luminescence properties. To achieve this goal, we have selected heterofunctional ligands, with a soft and a hard donor functionality, such as phosphines 2-pyridyldiphenylphosphine, 2-pyridylethyldiphenylphosphine, and bis(2-dipyridyl)phenylphosphine. These ligands coordinate to gold through the phosphorus atom and leave one or two free donor atoms for other metal centers. This kind of ligands have played an important role in the construction of homo and heterodinuclear complexes as exemplified by the use of 2-pyridylphenylphosphine.[10] The challenge here is to prepare a variety of complexes starting from the gold species [AuCl(P−N)] and different metal centers such as Cu(I), Rh(I), Ir(I), Pd(II), or Pt(II) and observe the trends, not only on the structural frameworks and coordination modes but also on the associated luminescence properties. These may be modified by the influence of the heterometallic ligand on the electronic spectra transitions and the states leading to emission. Density functional theory (DFT) and time dependent DFT (TD-DFT) studies have been carried out to complement the experimental studies and to interpret the results.

Results and Discussion

The reaction of the gold complex [AuCl(tht)] with heterofunctional phosphine ligands such as PPh_2py, $PPh_2CH_2CH_2py$, or $PPhpy_2$ gives the gold-phosphine metalloligands [AuCl(P−N)] (P−N = PPh_2py (**1**), $PPh_2CH_2CH_2py$ (**2**), $PPhpy_2$ (**3**)) (eq 1).

$$[AuCl(tht)] + P\text{-}N \longrightarrow [AuCl(P\text{-}N)] + tht \quad (1)$$

P-N = PPh_2py (**1**), $PPh_2CH_2CH_2py$ (**2**), $PPhpy_2$ (**3**)

Complexes **1**[11a] and **3**[11b] have been previously prepared. For complex **2** the $^{31}P\{^1H\}$ NMR spectrum shows the presence of only one phosphorus resonance at 29.52 ppm.

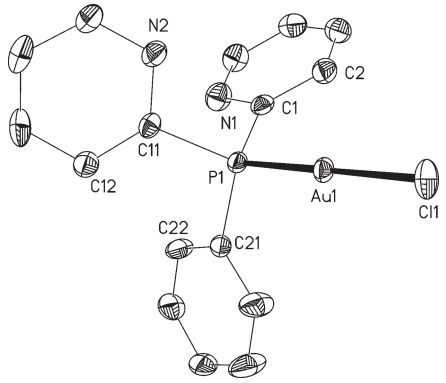

Figure 1. Structure of complex **3** showing the atom numbering scheme. Displacement parameter ellipsoids represent 50% probability surfaces. H atoms are omitted for clarity.

Table 1. Bond Lengths [Å] and Angles [deg] for Complex **3**

Au(1)−P(1)	2.2316(8)	C(1)−N(1)	1.366(4)
Au(1)−Cl(1)	2.2853(8)	C(5)−N(1)	1.354(5)
P(1)−C(21)	1.814(3)	C(11)−N(2)	1.352(4)
P(1)−C(1)	1.817(3)	C(15)−N(2)	1.347(4)
P(1)−C(11)	1.823(3)		
P(1)−Au(1)−Cl(1)	178.40(3)	N(1)−C(5)−C(4)	122.0(4)
C(21)−P(1)−C(1)	107.02(15)	C(5)−N(1)−C(1)	118.7(3)
C(21)−P(1)−C(11)	106.98(15)	N(2)−C(11)−C(12)	124.1(3)
C(1)−P(1)−C(11)	102.35(15)	N(2)−C(11)−P(1)	111.5(2)
C(21)−P(1)−Au(1)	111.92(11)	C(12)−C(11)−P(1)	124.3(3)
C(1)−P(1)−Au(1)	112.83(11)	N(2)−C(15)−C(14)	123.3(4)
C(11)−P(1)−Au(1)	114.99(11)	C(15)−N(2)−C(11)	116.4(3)
N(1)−C(1)−C(2)	121.1(3)	C(22)−C(21)−P(1)	120.9(3)
N(1)−C(1)−P(1)	118.2(3)	C(26)−C(21)−P(1)	118.2(3)
C(2)−C(1)−P(1)	120.7(3)		

In the ^1H NMR spectra, the resonances of the phenyl and pyridine protons are observed, as well as two multiplets for the methylene groups. Complex **1** has been structurally characterized previously by Alcock et al.[11c] The structure of complex **3** has been established by X-ray diffraction and is shown in Figure 1. A selection of bond lengths and angles are collected in Table 1. The coordination around the gold center is linear with a Cl−Au−P angle of 178.40(3)°, and bond distances Au−P of 2.2316(8) Å and Au−Cl of 2.2853(8) Å. There are no short intermolecular aurophilic contacts in contrast to those found in complex **1**. However, there are several Au···H and Cl···H short contacts that can be classified as hydrogen bonds.

In these complexes the heterofunctional phosphine ligands have pyridine groups that can be used to coordinate to other metal centers. Thus the reaction of complexes **1**−**3** with the copper(I) species $[Cu(NCMe)_4]X$ in a molar ratio 2:1 gives the trinuclear derivatives $[Au_2CuCl_2(P-N)_2]X$ (P−N = PPh_2py, X = BF_4 (**4**); $PPh_2CH_2CH_2py$, X = PF_6 (**5**); $PPhpy_2$, X = BF_4 (**6**)) according to the Scheme 1.

The crystal structure of complex **4** has been established by X-ray diffraction and is shown in Figure 2. A selection of bond lengths and angles are collected in Table 2. The structure is based on a triangular Au_2Cu cluster with an aurophilic Au(1)−Au(2) contact of 3.0658(5) Å, and Au(1)···Cu(1) and Au(2)···Cu(1) contacts of 2.9827(11) Å and 3.0485(11) Å, respectively. The copper atom is also bonded to the nitrogen atoms of the pyridine groups with distances Cu(1)−N(1) and Cu(1)−N(2) of 1.892(8) Å and 1.888(8) Å. The gold centers have a linear geometry slightly distorted because of the

(8) (a) Lefebvre, J.; Batchelor, R. J.; Leznoff, D. B. *J. Am. Chem. Soc.* **2004**, *126*, 16117–16125. (b) Katz, M. J.; Sakai, K.; Leznoff, D. B. *Chem. Soc. Rev.* **2008**, *37*, 1884–1895.

(9) (a) Wang, Q. M.; Lee, Y. A.; Crespo, O.; Deaton, J.; Tang, C.; Gysling, H. J.; Gimeno, M. C.; Larraz, C.; Villacampa, M. D.; Laguna, A.; Eisenberg, R. *J. Am. Chem. Soc.* **2004**, *126*, 9488–9489. (b) Crespo, O.; Gimeno, M. C.; Laguna, A.; Larraz, C.; Villacampa, M. D. *Chem.—Eur. J.* **2007**, *13*, 235–246.

(10) (a) Farr, J. P.; Olmstead, M. M.; Balch, A. L. *J. Am. Chem. Soc.* **1980**, *21*, 6654–6656. (b) Farr, J. P.; Olmstead, M. M.; Hunt, C. H.; Balch, A. L. *Inorg. Chem.* **1981**, *20*, 1182–1187. (c) McNair, R. J.; Nilsson, P. V.; Pignolet, L. H. *Inorg. Chem.* **1985**, *24*, 1935–1939. (d) Olmos, M. E.; Schier, A.; Schmidbaur, H. *Z. Naturforsch., B: Chem. Sci.* **1997**, *52*, 203–208. (e) Farr, J. P.; Olmstead, M. P.; Wood, F. E.; Balch, A. L. *J. Am. Chem. Soc.* **1983**, *105*, 792–798.

(11) (a) Ang, H. G.; Know, W. E.; Mok, K. F. *Inorg. Nucl. Chem. Lett.* **1972**, *8*, 829–832. (b) Inoguchi, Y.; Milewski-Mahrla, B.; Schmidbaur, H. *Chem. Ber.* **1982**, *115*, 3085–3095. (c) Alcock, N. W.; Moore, P.; Lampe, P. A.; Mok, K. F. *J. Chem. Soc., Dalton Trans.* **1982**, 207–210.

Scheme 1

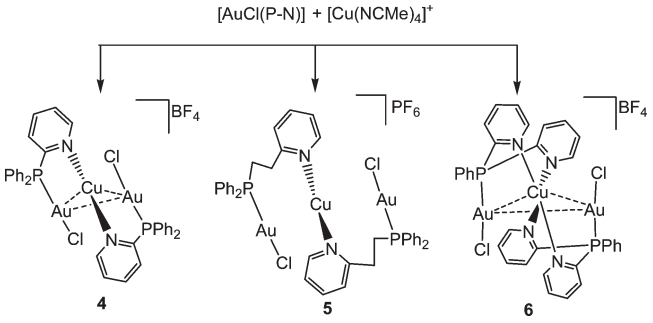

Table 2. Bond Lengths [Å] and Angles [deg] for Complex **4**

Au(1)−P(1)	2.226(2)	Au(2)−Cl(2)	2.297(2)
Au(1)−Cl(1)	2.296(2)	Au(2)−Cu(1)	3.0485(11)
Au(1)−Cu(1)	2.9827(11)	Cu(1)−N(2)	1.888(8)
Au(1)−Au(2)	3.0658(5)	Cu(1)−N(1)	1.892(8)
Au(2)−P(2)	2.233(2)		
P(1)−Au(1)−Cl(1)	174.10(8)	P(2)−Au(2)−Au(1)	103.19(6)
P(1)−Au(1)−Cu(1)	71.80(6)	Cl(2)−Au(2)−Au(1)	82.64(6)
Cl(1)−Au(1)−Cu(1)	113.98(6)	Cu(1)−Au(2)−Au(1)	58.39(2)
P(1)−Au(1)−Au(2)	100.60(6)	N(2)−Cu(1)−N(1)	176.1(3)
Cl(1)−Au(1)−Au(2)	83.76(5)	N(2)−Cu(1)−Au(1)	84.0(2)
Cu(1)−Au(1)−Au(2)	60.51(2)	N(1)−Cu(1)−Au(1)	94.3(2)
P(2)−Au(2)−Cl(2)	172.97(8)	N(2)−Cu(1)−Au(2)	91.7(2)
P(2)−Au(2)−Cu(1)	70.29(6)	N(1)−Cu(1)−Au(2)	84.4(2)
Cl(2)−Au(2)−Cu(1)	116.50(6)	Au(1)−Cu(1)−Au(2)	61.09(2)

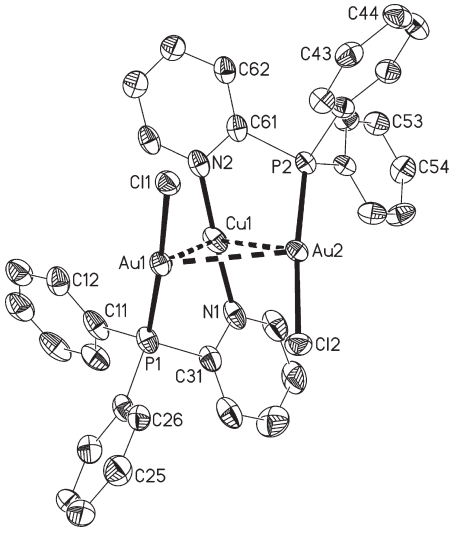

Figure 2. Structure of complex **4** showing the atom numbering scheme. Displacement parameter ellipsoids represent 50% probability surfaces. H atoms are omitted for clarity.

presence of metal···metal short contacts, with the P(2)−Au(2)−Cl(2) angle being 172.97(8)°, and P(1)−Au(1)−Cl(1) 174.10(8)°. The N(2)−Cu(1)−N(1) angle is 176.1(3)°, which defines a linear geometry for the Cu atom, distorted also by the metal close proximity to the other metals.

These complexes have different colors, namely, complex **4** is yellow, complex **5** is white, and complex **6** orange. The copper center is probably bonded in all complexes to the nitrogen atoms of the heterofunctional phosphine ligands, and the color can be indicative of the presence of Au···Cu interactions, which should be favored in complexes **4** and **6** but not in complex **5** because of the longer chain of the phosphine ligand. In complex **6** it is likely that the four pyridine

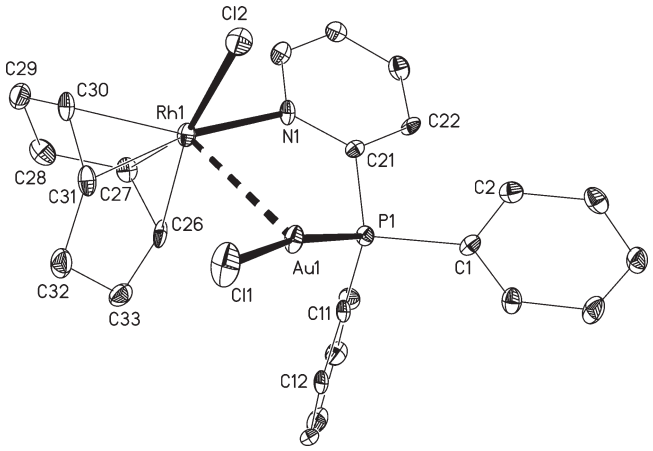

Figure 3. Structure of complex **7** showing the atom numbering scheme. Displacement parameter ellipsoids represent 30% probability surfaces. H atoms are omitted for clarity.

groups form four covalent Cu−N bonds, defining a tetrahedral coordination of Cu(I), different from the linear coordination observed in complex **4**, where only two pyridine groups are present in the ligands. This coordination is corroborated by NMR spectroscopy in solution and thus the ^{1}H NMR spectrum shows equivalent pyridine protons for all the complexes even at low temperature. The $^{31}P\{^{1}H\}$ NMR spectra show in all the cases one unique resonance indicating the equivalence of the phosphorus atoms.

We have also studied the reaction of complexes **1**−**3** with $[M(\mu\text{-Cl})(cod)]_2$ (M = Rh or Ir) in a 2:1 molar ratio. The results depend on the phosphine used. When the phosphine ligand is PPh_2py, the dinuclear complexes with Au···Rh or Au···Ir short contacts are obtained (eq 2).

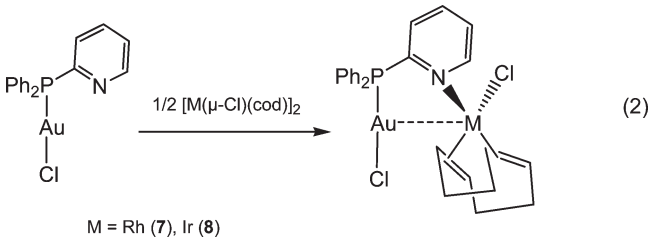

(2)

The ^{1}H NMR spectra show the protons corresponding to the phosphine and cycloctadiene (cod); the olefinic protons appear around 4 ppm whereas the alkyl ones appear around 2.5 and 1.7 ppm. The $^{31}P\{^{1}H\}$ NMR spectra show only one resonance for the phosphorus atom. The structures of complexes **7** and **8** have been established by X-ray diffraction and are shown in Figures 3 and 4. A selection of bond lengths and angles are presented in Tables 3 and 4. They have intermetallic distances Au···Rh of 3.0385(9) Å or Au···Ir of 3.0148(4) Å. The geometry of the gold atom is distorted from linear, with P−Au−Cl angles of 169.59(8)° for the rhodium complex and 169.28(7)° for the iridium derivative, which may be a consequence of the metal···metal short contacts. The Rh and Ir centers have a square-planar geometry, the narrower angles being N(1)−Rh(I)−Cl(2) of 86.12(19)° and N(1)−Ir(1)−Cl(2) of 86.99(15)°. The Rh−N distances of 2.118(6) Å and Ir−N of 2.109(5) Å are similar to other M−N bonds in Rh(I) or Ir(I) complexes, respectively.[10a,12]

(12) Drury, W. J., III; Zimmermann, N.; Keenan, M.; Hayashi, M.; Kaiser, S.; Goddard, R.; Pfaltz, A. *Angew. Chem., Int. Ed.* **2004**, *43*, 70–74.

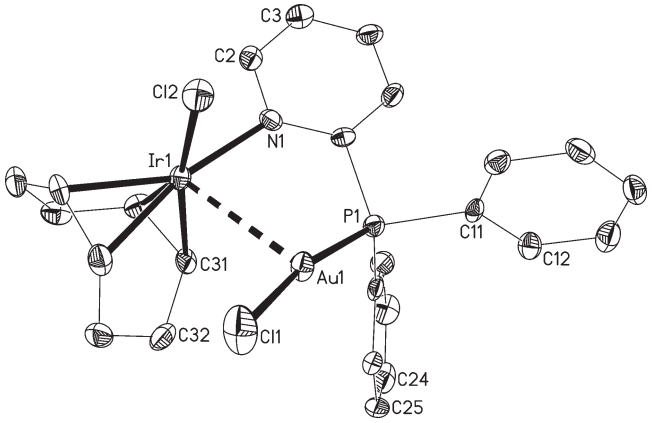

Figure 4. Structure of complex **8** showing the atom numbering scheme. Displacement parameter ellipsoids represent 50% probability surfaces. H atoms are omitted for clarity.

Table 3. Bond Lengths [Å] and Angles [deg] for Complex **7**

Au(1)−P(1)	2.223(2)	Rh(1)−C(31)	2.154(7)
Au(1)−Cl(1)	2.308(2)	Rh(1)−Cl(2)	2.374(2)
Au(1)−Rh(1)	3.0385(9)	P(1)−C(1)	1.812(8)
Rh(1)−N(1)	2.118(6)	P(1)−C(11)	1.823(8)
Rh(1)−C(30)	2.135(7)	P(1)−C(21)	1.835(8)
Rh(1)−C(27)	2.135(8)	C(21)−N(1)	1.358(9)
Rh(1)−C(26)	2.140(8)	C(25)−N(1)	1.349(10)
P(1)−Au(1)−Cl(1)	169.59(8)	C(27)−Rh(1)−Cl(2)	157.8(2)
P(1)−Au(1)−Rh(1)	81.95(6)	C(26)−Rh(1)−Cl(2)	163.8(2)
Cl(1)−Au(1)−Rh(1)	108.13(6)	C(31)−Rh(1)−Cl(2)	95.5(2)
N(1)−Rh(1)−C(30)	153.3(3)	N(1)−Rh(1)−Au(1)	86.49(17)
N(1)−Rh(1)−C(27)	93.8(3)	C(30)−Rh(1)−Au(1)	117.2(2)
C(30)−Rh(1)−C(27)	81.1(3)	C(27)−Rh(1)−Au(1)	128.4(2)
N(1)−Rh(1)−C(26)	93.9(3)	C(26)−Rh(1)−Au(1)	90.0(2)
C(30)−Rh(1)−C(26)	97.8(3)	C(31)−Rh(1)−Au(1)	83.4(2)
C(27)−Rh(1)−C(26)	38.4(3)	Cl(2)−Rh(1)−Au(1)	73.75(6)
N(1)−Rh(1)−C(31)	168.9(3)	C(25)−N(1)−Rh(1)	114.1(5)
C(30)−Rh(1)−C(31)	37.8(3)	C(21)−N(1)−Rh(1)	128.4(5)
C(27)−Rh(1)−C(31)	88.8(3)	C(27)−C(26)−Rh(1)	70.6(5)
C(26)−Rh(1)−C(31)	81.4(3)	C(33)−C(26)−Rh(1)	111.1(6)
N(1)−Rh(1)−Cl(2)	86.12(19)	C(26)−C(27)−Rh(1)	71.0(4)
C(30)−Rh(1)−Cl(2)	89.0(2)	C(28)−C(27)−Rh(1)	113.8(6)
C(31)−C(30)−Rh(1)	71.8(4)	C(30)−C(31)−Rh(1)	70.3(4)
C(29)−C(30)−Rh(1)	109.2(5)	C(32)−C(31)−Rh(1)	111.7(5)

Table 4. Selected Bond Lengths [Å] and Angles [deg] for Complex **8**

Au(1)−P(1)	2.2213(16)	Ir(1)−C(38)	2.129(7)
Au(1)−Cl(1)	2.3063(17)	Ir(1)−C(35)	2.133(6)
Au(1)−Ir(1)	3.0148(4)	Ir(1)−C(34)	2.136(6)
Ir(1)−C(31)	2.099(6)	Ir(1)−Cl(2)	2.3561(17)
Ir(1)−N(1)	2.109(5)		
P(1)−Au(1)−Cl(1)	169.28(7)	C(35)−Ir(1)−C(34)	39.2(3)
P(1)−Au(1)−Ir(1)	82.44(4)	C(31)−Ir(1)−Cl(2)	164.67(18)
Cl(1)−Au(1)−Ir(1)	108.14(5)	N(1)−Ir(1)−Cl(2)	86.99(15)
C(31)−Ir(1)−N(1)	92.6(2)	C(38)−Ir(1)−Cl(2)	156.33(19)
C(31)−Ir(1)−C(38)	39.0(2)	C(35)−Ir(1)−Cl(2)	88.65(19)
N(1)−Ir(1)−C(38)	92.4(2)	C(34)−Ir(1)−Cl(2)	96.1(2)
C(31)−Ir(1)−C(35)	98.4(3)	C(31)−Ir(1)−Au(1)	89.74(18)
N(1)−Ir(1)−C(35)	152.9(2)	N(1)−Ir(1)−Au(1)	86.90(14)
C(38)−Ir(1)−C(35)	81.2(3)	C(38)−Ir(1)−Au(1)	128.69(18)
C(31)−Ir(1)−C(34)	81.3(3)	C(35)−Ir(1)−Au(1)	117.64(18)
N(1)−Ir(1)−C(34)	167.8(2)	C(34)−Ir(1)−Au(1)	82.55(19)
C(38)−Ir(1)−C(34)	89.5(3)	Cl(2)−Ir(1)−Au(1)	74.93(4)

The reaction of $[AuCl(PPh_2CH_2CH_2py)]$ with $[M(\mu\text{-}Cl)(cod)]_2$ (M = Rh, Ir) in a 2:1 molar ratio gives yellow solids of complexes **9** and **10**. The conductivity measurements indicate that the compounds are conductors.

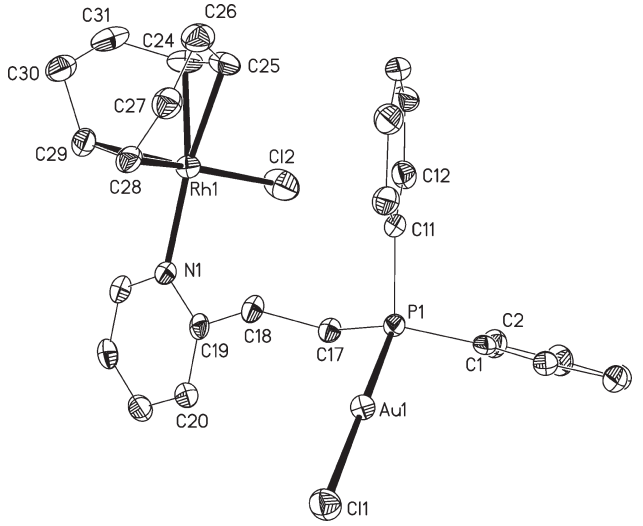

Figure 5. Structure of complex **9** showing the atom numbering scheme. Displacement parameter ellipsoids represent 50% probability surfaces. H atoms are omitted for clarity.

Table 5. Selected Bond Lengths [Å] and Angles [deg] for Complex **9**

Au(1)−P(1)	2.2393(16)	Rh(1)−C(24)	2.123(5)
Au(1)−Cl(1)	2.2913(16)	Rh(1)−C(29)	2.138(5)
Rh(1)−N(1)	2.108(4)	Rh(1)−C(25)	2.152(5)
Rh(1)−C(28)	2.121(5)	Rh(1)−Cl(2)	2.3809(17)
P(1)−Au(1)−Cl(1)	178.37(5)	C(28)−Rh(1)−C(25)	82.2(2)
N(1)−Rh(1)−C(28)	91.34(18)	C(24)−Rh(1)−C(25)	37.8(2)
N(1)−Rh(1)−C(24)	156.0(2)	C(29)−Rh(1)−C(25)	89.8(2)
C(28)−Rh(1)−C(24)	98.9(2)	N(1)−Rh(1)−Cl(2)	88.31(12)
N(1)−Rh(1)−C(29)	92.67(19)	C(28)−Rh(1)−Cl(2)	157.10(15)
C(28)−Rh(1)−C(29)	38.4(2)	C(24)−Rh(1)−Cl(2)	90.41(18)
C(24)−Rh(1)−C(29)	82.4(2)	C(29)−Rh(1)−Cl(2)	164.44(15)
N(1)−Rh(1)−C(25)	166.19(19)	C(25)−Rh(1)−Cl(2)	92.91(17)

The structure of complex **9** has been confirmed by X-ray diffraction and shown to be a dinuclear molecule as depicted in Figure 5. Selected bond lengths and angles are collected in Table 5. The complex crystallizes with a water molecule. Gold−rhodium interactions are prevented by the relative orientation between the two metals, as might be expected owing to the long chain of the functionalized phosphine. The gold center has a linear coordination with a Cl−Au−P angle of 178.37(5)°, whereas the rhodium center displays a square planar geometry, distorted because of the bite angle of the cycloctadiene ligand, C−Rh−C 82.4(2)° or 82.2(2)°. The Rh−N distance is 2.108(4) Å, which is of the same order than that in complex **7**. There are several Cl···H short contacts about 2.8 Å, which can be classified as hydrogen bonds; one of them involves the hydrogen from the water molecule with a distance Cl2−H0 of 2.581 Å.

This crystal structure of complex **9** confirms the same structural pattern observed in compounds **7** and **8**. However, the NMR data of complexes **9** and **10** do not agree with this structure as they show a structural pattern different from that of complexes **7** and **8**, with two inequivalent phosphine and cycloctadiene ligands. In the ^1H NMR spectra, the resonances corresponding to two different pyridine groups and two cyclooctadiene ligands are observed; furthermore all the protons of the cyclooctadiene ligands appear as inequivalent. In the $^{31}P\{^1H\}$ NMR spectra two resonances are observed for each complex, with a chemical shift characteristic of phosphorus bonded to gold, namely, 32.41 and 29.49 ppm for the

Scheme 2

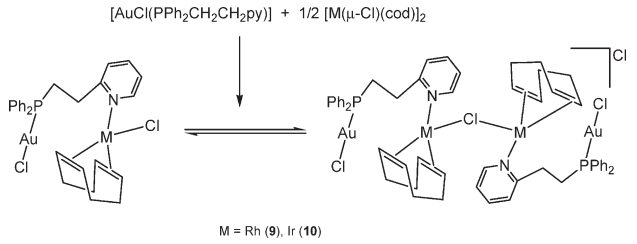

Scheme 3

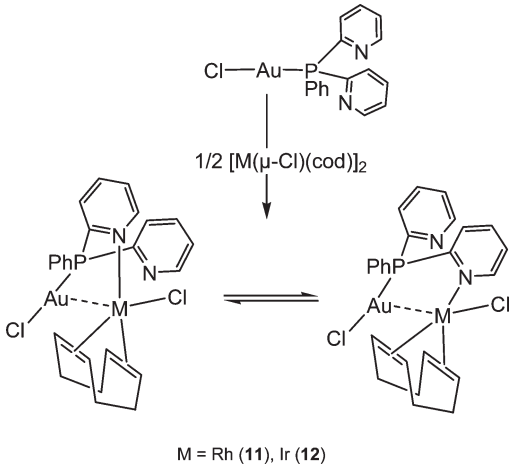

Rh complex, and 32.38 and 29.69 ppm for the Ir one. No coupling between rhodium and phosphorus is observed. Furthermore, the coordination of the phosphine to rhodium or iridium does not take place because the chemical shift is not characteristic of these types of bonds, and no coupling with the rhodium atom is observed. We thus propose that one dinuclear unit loses a chloride ligand in solution. The unsaturated Rh or Ir atoms will then bind the chloride of a second unit, to give a tetranuclear arrangement with only one bridging chloride (such species are not new in the chemistry of these metals).[13] The other coordination positions around the rhodium or iridium centers are occupied by the cod and the pyridine ligands, while the dissociated chlorine acts as counterion. The observation of signals from two phosphine and two cyclooctadiene ligands in the NMR spectra could arise from the equilibrium between both species (see Scheme 2).

The treatment of $[AuCl(PPhpy_2)]$ with $[M(\mu\text{-}Cl)(cod)]_2$ (M = Rh, Ir), in a molar ratio 2:1, leads to the dinuclear derivatives **11** and **12** in which the rhodium or iridium centers are coordinated to one of the pyridine units from the phosphine ligand (Scheme 3). In the ^{1}H NMR spectrum of complex **11** only one resonance for each type of protons of the pyridine is observed, which can arise from a rapid interchange between the pyridines coordinated to the rhodium center. At low temperature, two types of pyridine groups are observed, and the protons of the cyclooctadiene ligand also become nonequivalent. The ^{1}H NMR spectrum of a solution of a crystalline sample of complex **12** shows at room temperature two types of pyridine groups. The ^{31}P{^{1}H} NMR spectra show in both complexes a single resonance for the phosphorus atom.

(13) (a) Wachter, J.; Jeanneaux, F.; Le Borgne, G.; Riess, J. G. *Organometallics* **1984**, *3*, 1034–1038. (b) Broussier, R.; Laly, M.; Perron, P.; Gautheron, B.; Nifant'ev, I. E.; Howard, J. A. K.; Kuz'mina, L. G.; Kalck, P. *J. Organomet. Chem.* **1999**, *587*, 104–112. (c) Cuervo, D.; Diez, J.; Gamasa, M. P.; Gimeno, J. *Organometallics* **2005**, *24*, 2224–2232.

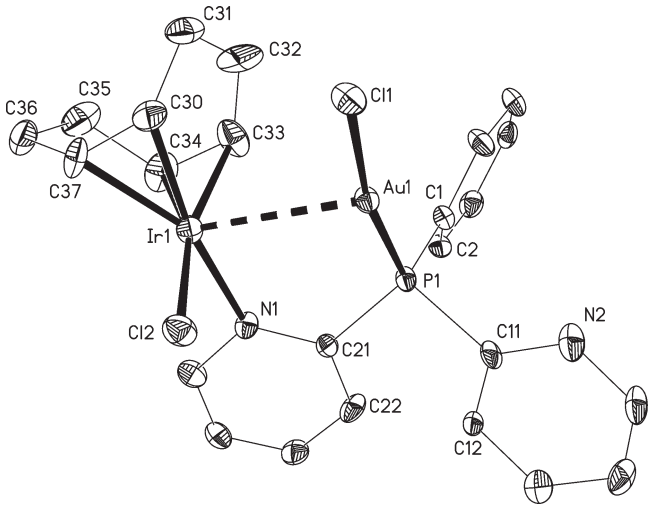

Figure 6. Structure of complex **12** showing the atom numbering scheme. Displacement parameter ellipsoids represent 30% probability surfaces. H atoms are omitted for clarity.

Table 6. Selected Bond Lengths [Å] and Angles [deg] for Complex **12**

Au(1)−P(1)	2.216(3)	Au(2)−P(2)	2.221(3)
Au(1)−Cl(1)	2.307(3)	Au(2)−Cl(3)	2.300(3)
Au(1)−Ir(1)	3.0417(10)	Au(2)−Ir(2)	3.0427(11)
Ir(1)−N(1)	2.088(10)	Ir(2)−C(77)	2.096(13)
Ir(1)−C(34)	2.097(15)	Ir(2)−N(3)	2.105(10)
Ir(1)−C(30)	2.108(14)	Ir(2)−C(70)	2.127(13)
Ir(1)−C(33)	2.137(16)	Ir(2)−C(73)	2.127(13)
Ir(1)−C(37)	2.150(14)	Ir(2)−C(74)	2.162(13)
Ir(1)−Cl(2)	2.359(4)	Ir(2)−Cl(4)	2.370(3)
P(1)−Au(1)−Cl(1)	169.88(12)	N(1)−Ir(1)−Cl(2)	87.8(3)
P(1)−Au(1)−Ir(1)	81.92(8)	C(34)−Ir(1)−Cl(2)	160.8(5)
Cl(1)−Au(1)−Ir(1)	107.99(10)	C(30)−Ir(1)−Cl(2)	94.2(5)
N(1)−Ir(1)−C(34)	90.7(6)	C(33)−Ir(1)−Cl(2)	161.9(4)
N(1)−Ir(1)−C(30)	170.5(5)	C(37)−Ir(1)−Cl(2)	90.5(4)
C(34)−Ir(1)−C(30)	90.5(7)	N(1)−Ir(1)−Au(1)	88.6(3)
N(1)−Ir(1)−C(33)	93.7(6)	C(34)−Ir(1)−Au(1)	122.8(5)
C(34)−Ir(1)−C(33)	37.3(6)	C(30)−Ir(1)−Au(1)	82.9(4)
C(30)−Ir(1)−C(33)	81.6(7)	C(33)−Ir(1)−Au(1)	85.7(4)
N(1)−Ir(1)−C(37)	153.7(5)	C(37)−Ir(1)−Au(1)	116.5(4)
C(34)−Ir(1)−C(37)	82.4(6)	Cl(2)−Ir(1)−Au(1)	76.29(9)
C(30)−Ir(1)−C(37)	35.7(6)	P(2)−Au(2)−Cl(3)	168.59(12)
C(33)−Ir(1)−C(37)	96.0(7)	P(2)−Au(2)−Ir(2)	80.48(9)
Cl(3)−Au(2)−Ir(2)	110.77(9)	C(77)−Ir(2)−Cl(4)	162.4(4)
C(77)−Ir(2)−N(3)	93.1(5)	N(3)−Ir(2)−Cl(4)	87.4(3)
C(77)−Ir(2)−C(70)	39.1(5)	C(70)−Ir(2)−Cl(4)	158.5(4)
N(3)−Ir(2)−C(70)	92.2(5)	C(73)−Ir(2)−Cl(4)	89.3(4)
C(77)−Ir(2)−C(73)	97.9(5)	C(74)−Ir(2)−Cl(4)	95.7(4)
N(3)−Ir(2)−C(73)	153.2(4)	C(77)−Ir(2)−Au(2)	87.4(3)
C(70)−Ir(2)−C(73)	81.4(5)	N(3)−Ir(2)−Au(2)	89.4(3)
C(77)−Ir(2)−C(74)	80.4(5)	C(70)−Ir(2)−Au(2)	126.5(4)
N(3)−Ir(2)−C(74)	167.9(5)	C(73)−Ir(2)−Au(2)	115.3(3)
C(70)−Ir(2)−C(74)	89.2(5)	C(74)−Ir(2)−Au(2)	80.1(4)
C(73)−Ir(2)−C(74)	38.8(5)	Cl(4)−Ir(2)−Au(2)	75.01(8)

The crystal structure of complex **12** has been determined by X-ray diffraction and is shown in Figure 6. A selection of bond lengths and angles are collected in Table 6. The complex crystallizes with two independent molecules per asymmetric unit. There is an intermetallic Au···Ir distance of 3.0417(10) Å, which is similar to that found in complex **8**. The geometry around the gold atom is slightly distorted from linearity, with a P−Au−Cl angle of 169.88(12)°, probably to allow the gold−iridium interaction. The iridium center is in a square planar geometry with the angle N(1)−Ir(1)−Cl(2) being

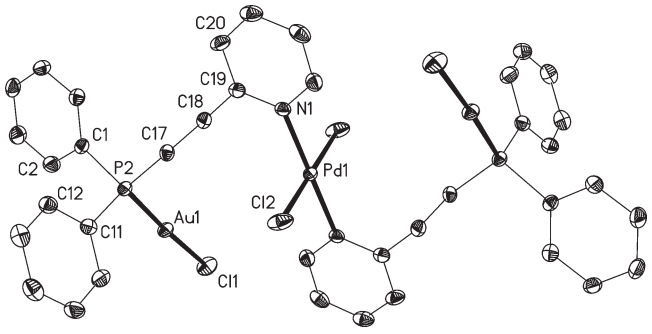

Figure 7. Structure of complex **13** showing the atom numbering scheme. Displacement parameter ellipsoids represent 50% probability surfaces. H atoms are omitted for clarity.

Table 7. Selected Bond Lengths [Å] and Angles [deg] for Complex **13**[a]

Au(1)−P(2)	2.2233(10)	Pd(1)−Cl(2)	2.2942(10)
Au(1)−Cl(1)	2.2846(10)	P(2)−C(11)	1.803(4)
Pd(1)−N(1)	2.027(3)	P(2)−C(1)	1.808(4)
Pd(1)−N(1)#1	2.027(3)	P(2)−C(17)	1.817(4)
P(2)−Au(1)−Cl(1)	177.01(4)	C(1)−P(2)−C(17)	107.73(18)
N(1)−Pd(1)−N(1)#1	180.0(3)	C(11)−P(2)−Au(1)	114.87(14)
N(1)−Pd(1)−Cl(2)	90.25(9)	C(1)−P(2)−Au(1)	113.00(13)
N(1)#1-Pd(1)−Cl(2)	89.75(9)	C(17)−P(2)−Au(1)	111.84(13)
Cl(2)−Pd(1)−Cl(2)#1	180.00(6)	C(19)−N(1)−Pd(1)	123.6(3)
C(11)−P(2)−C(1)	106.20(18)	C(23)−N(1)−Pd(1)	117.0(3)
C(11)−P(2)−C(17)	102.42(18)		

[a] Symmetry transformations used to generate equivalent atoms: #1, $-x+1/2,-y+1/2,-z$; #2, $-x+2,y,-z+1/2$.

87.8(3)°. The Ir−N bond distance is 2.088(10) Å, which is slightly shorter than in the derivative with the PPh_2py ligand.

We have also studied the reactivity of the complexes [AuCl(P−N)] toward palladium or platinum derivatives such as $[MCl_2(NCPh)_2]$ (M = Pd, Pt), in a molar ratio 2:1. We have obtained the expected trinuclear complexes as pale yellow solids, with the exception of M = Pd and P−N = PPh_2py, for which a mixture of complexes has been obtained. The preparation of the complexes is shown in eq 3, and the Pd or Pt atoms are coordinated to pyridine groups with a *trans* disposition (see X-ray structure of complex **13**, Figure 7).

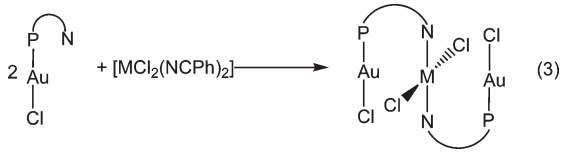

(P-N) = $PPh_2CH_2CH_2py$ (**13**), $PPhpy_2$ (**14**); M = Pd

(P-N) = PPh_2py (**15**), $PPh_2CH_2CH_2py$ (**16**), $PPhpy_2$ (**17**); M = Pt

In the ^1H spectra of complexes **13**−**17**, only some of the protons of the pyridine moieties are resolved because the rest overlap with the phenyl protons. When the phosphine ligand is $PPh_2CH_2CH_2py$, the methylene protons show resonances at 4.20 and 3.35 ppm, for the palladium complex **13**, and at 3.26 and 3.15 ppm for the platinum derivative **16**. The $^{31}P\{^1H\}$ NMR spectra of these complexes show only one resonance for the equivalent phosphorus atoms.

The structure of complex **13** has been confirmed by X-ray diffraction studies, and the molecule is shown in Figure 7. A selection of bond lengths and angles are collected in Table 7. The complex crystallizes as the *trans* isomer, as expected because of its higher stability compared to the *cis* isomer. The molecule has a symmetry center and only half corresponds to the asymmetric unit. The geometry around the gold centers is linear with a Cl−Au−P angle of 177.01(4)°. There are no Au···Pd short contacts, probably because of the longer backbone chain of this heterofunctional phosphine. The palladium center is found in a regular square planar geometry with the angles very close to 90°.

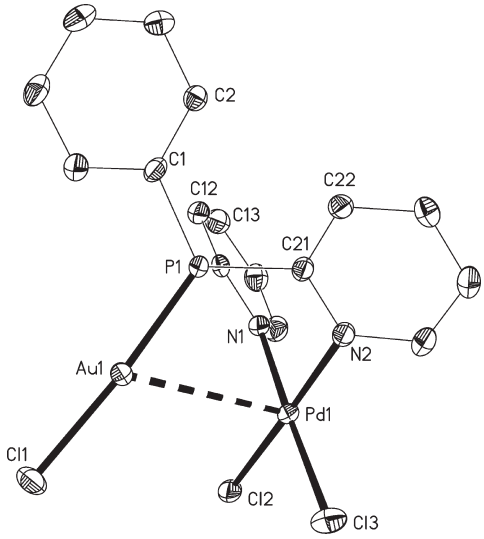

Figure 8. Structure of complex **18** showing the atom numbering scheme. Displacement parameter ellipsoids represent 50% probability surfaces. H atoms are omitted for clarity.

Table 8. Selected Bond Lengths [Å] and Angles [deg] for Complex **18**

Au(1)−P(1)	2.2255(8)	Pd(1)−N(1)	2.040(2)
Au(1)−Cl(1)	2.2790(8)	Pd(1)−Cl(2)	2.2934(9)
Au(1)−Pd(1)	3.2010(7)	Pd(1)−Cl(3)	2.2936(10)
Pd(1)−N(2)	2.035(2)		
P(1)−Au(1)−Cl(1)	172.10(3)	N(1)−Pd(1)−Cl(3)	177.88(7)
P(1)−Au(1)−Pd(1)	67.256(19)	Cl(2)−Pd(1)−Cl(3)	91.80(4)
Cl(1)−Au(1)−Pd(1)	114.49(2)	N(2)−Pd(1)−Au(1)	88.42(6)
N(2)−Pd(1)−N(1)	87.85(9)	N(1)−Pd(1)−Au(1)	83.65(7)
N(2)−Pd(1)−Cl(2)	177.53(7)	Cl(2)−Pd(1)−Au(1)	91.55(2)
N(1)−Pd(1)−Cl(2)	89.69(7)	Cl(3)−Pd(1)−Au(1)	97.81(2)
N(2)−Pd(1)−Cl(3)	90.65(7)		

Finally, we tried the reaction of $[AuCl(PPhpy_2)]$ with *trans*-$[PdCl_2(NCPh)_2]$ in a molar ratio 1:1. Since the phosphine ligand has two pyridine groups available for bonding, the expected result should be the coordination of the two pyridine moieties to the palladium center affording a dinuclear derivative as shown in eq 4.

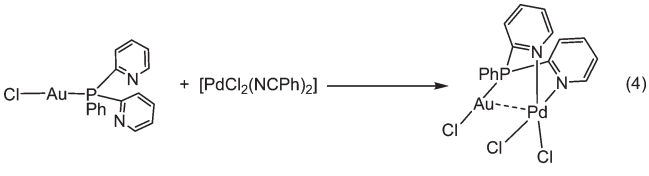

18

Complex **18** is a yellow air- and moisture-stable solid. The ^1H NMR spectrum shows the four broad resonances for the two pyridine groups, whereas the $^{31}P\{^1H\}$ NMR spectrum presents one unique resonance for the phosphorus atoms.

The structure of complex **18** has been established by X-ray diffraction studies, and the molecule is shown in Figure 8. A selection of bond lengths and angles are collected in Table 8. In contrast with the structure of complex **13**, which possesses a long chain phosphine ligand, the structure of **18** presents a

Table 9. Maxima Observed in the DRUV Spectra of Complexes **1**−**18** in the Solid State at 298 K

compound	DRUV
[AuCl(PPh_2py)] (**1**)	< 300
[AuCl($PPh_2(CH_2)_2py_2$)] (**2**)	< 300
[AuCl($PPhpy_2$)] (**3**)	< 300
[$Au_2CuCl_2(\mu$-$PPh_2py)_2$]BF_4 (**4**)	270, 320, 405, 470−510
[$Au_2CuCl_2(\mu$-$PPh_2(CH_2)_2py_2)_2$]PF_6 (**5**)	210, 260, 330−400
[$Au_2CuCl_2(\mu$-$PPhpy_2)_2$]BF_4 (**6**)	270, 320, 405−550
[$AuRhCl_2(\mu$-PPh_2py)(cod)] (**7**)	250, 325, 410−500
[$AuIrCl_2(\mu$-PPh_2py)(cod)] (**8**)	250, 350, 450, 500−550
[$AuRhCl_2(\mu$-$PPh_2(CH_2)_2py_2$)(cod)] (**9**)[a]	250, 325, 410−500
[$AuIrCl_2(\mu$-$PPh_2(CH_2)_2py_2$)(cod)] (**10**)[a]	250, 350, 450, 500−600
[$AuRhCl_2(\mu$-$PPhpy_2)_2$(cod)] (**11**)	250, 325, 410−500
[$AuIrCl_2(\mu$-$PPhpy_2)_2$(cod)] (**12**)	250, 350, 450,500−600
[$Au_2PdCl_4(\mu$-$PPh_2(CH_2)_2py_2)_2$] (**13**)	250, 350, 450, 500
[$Au_2PdCl_4(\mu$-$PPhpy_2)_2$] (**14**)	250, 350, 450, 500
[$Au_2PtCl_4(\mu$-$PPh_2py)_2$] (**15**)	270, 310−500
[$Au_2PtCl_4(\mu$-$PPh_2(CH_2)_2py_2)_2$] (**16**)	270, 310−400
[$Au_2PtCl_4(\mu$-$PPhpy_2)_2$] (**17**)	270, 310−400
[$AuPdCl_3(\mu$-$PPhpy_2)$] (**18**)	270, 320, 405, 470−510

[a] This complex could be a mixture of both present in solution.

short Au···Pd distance of 3.2010(7) Å, which can indicate a weak bonding interaction. The geometries around the gold and palladium atoms are linear and square-planar, respectively, only with slight deviations from the ideal geometries. The chloride ligands around the palladium center are in a mutually *cis* disposition.

Diffuse Reflectance UV Studies. The diffuse-reflectance UV (DRUV) spectra of the metalloligands (**1**−**3**) in the solid state display bands with maxima at $\lambda < 300$ nm (see Table 9). Upon coordination of heterometallic atoms to **1**−**3**, broad bands appear at $\lambda \geq 400$ nm. For compounds **5**, **16**, and **17** the lowest energy band reaches 400 nm, but in most of the cases it reaches 500 nm and even 600 nm (complexes **10** and **12**). Intense absorptions at about 266 nm (shoulder at 275 nm) have been attributed to PPh_2py intraligand (IL) transitions ($\pi \rightarrow \pi^*$ or $n \rightarrow \pi$)[14] in mixed phosphine-thiolate gold(I) complexes. The absorptions observed at lower energies in our complexes (which include those which lead to the emissions) could correspond to charge transfer processes between the metallic atom and the ligands, or to the presence of metallic interactions, as absorptions at 326 nm have been attributed to gold···copper interactions in the complex [{AuCu(Spy)(PPh_2py)}$_2$]$(PF_6)_2$.[14]

Luminescence Studies. Upon excitation between 314 and 375 nm the free phosphines display an emission maximum at 554 nm (PPh_2py)[14] and 443 nm ($PPh_2CH_2CH_2py$) at room temperature, and at 529 nm (PPh_2py), 491 nm ($PPh_2CH_2CH_2py$), and 499 nm ($PPhpy_2$) at 77 K. The luminescent behavior of the complexes may be summarized in the following points: (i) None of the metalloligands **1**−**3** show luminescence at room temperature. At 77 K compounds **1** and **3** display an emission at 499 nm upon excitation at about 300 nm (see Table 10). (ii) The maxima of emission shown by the heterometallic Au/Cu complexes depend on the phosphine. (iii) All heterometallic Au/Ir complexes display luminescence except compound **10**, which contains the monophosphine with the longer chain ($PPh_2CH_2CH_2py$). (iv) The Au/Rh, Au/Pd, and Au/Pt complexes are not emissive.

For the discussion of the possible origin of these emissions we shall first analyze the metalloligands themselves and then the heterobimetallic systems.

The energies of the emissions for metalloligands **1** and **3** resemble those obtained for the monophosphines. Thus, IL transitions are probably responsible for the luminescence (IL, phosphine) in **1** and **3**.

The heterobimetallic systems exhibit different behavior. The Au/Cu species **4**−**6** are luminescent both at 298 and 77 K, but very weakly emissive at room temperature. The emission maxima for complexes **4** (P−N = PPh_2py) and **5** (P−N = $PPh_2CH_2CH_2py$) appear between 516 and 558 nm (excitation maxima between 320 and 410 nm). Broad bands are observed at room temperature, whereas at 77 K a band and a not well-defined shoulder are observed. Lifetime measurements for these complexes at room temperature [**4** 29 μs; **5** 13 μs] point to a phosphorescent nature of these emissions. The bands appear at energies similar to those described for the free phosphine, suggesting that they are not related to the presence of metallophilic interactions. IL transitions modified by the coordination to the copper center or MLCT (metal to ligand charge transfer)[15,16] could be responsible of these emissions. Complex **6** displays an emission at about 700 nm upon excitation at about 460 nm, both at 298 and 77 K. This emission is observed at much lower energy than in **4** and **5**. In CuN_4 systems with a coordination sphere similar to the one proposed for **6**, luminescence has been attributed to MLCT transitions.[15,16] The same explanation might be applied to **6**, although Au···Cu interactions are possible in this complex. Thus, the luminescent emissions of the bimetallic Cu/Au complexes **4**−**6** seem to be more influenced by the geometry around the copper center than by the presence or absence or Au···Cu interactions. The lower emission energy suggests the assignment of a tetrahedral environment copper atom in **6**, by comparison with other copper complexes with coordination CuN_4,[15,16] distinct from the linear one observed for **4** and proposed for **5**.

The Au/Ir derivatives **8** and **12** only emit at 77 K, displaying emissions with $\lambda_{max} > 608$ nm, while **10** does not display luminescence. For compound **12**, two maxima are observed which undergo changes in relative intensity when the emission excitation is modified. Upon excitation at 500 nm, the maximum at 711 increases its intensity, and excitation at 450 nm leads to a band, whose emission maximum appears at 620 nm, and to a shoulder. For these gold/iridium derivatives the luminescence properties are associated with the presence of Au···Ir interactions, observed in **8** and **12** but not expected in **10**. In other Au(I)/Ir(I)[17] systems the luminescence has been assigned to metal centered ($d\sigma^* \rightarrow p\sigma$) transitions. Despite the important role apparently played by the metallophilic interactions in the luminescent origin, from these data it is not possible to assign the nature of the transitions associated, since they might be metal centered, or metal charge transitions involving Au and/or Ir (MMLCT). On the

(14) Hao, L.; Mansour, M. A.; Lachicotte, R.; Gysling, H. J.; Eisenberg, R. *Inorg. Chem.* **2000**, *39*, 5520–5529.

(15) McMillin, D. R.; McNett, K. M. *Chem. Rev.* **1998**, *98*, 1201–1219.
(16) Patra, G. K.; Goldberg, I. *Eur. J. Inorg. Chem.* **2003**, 969–977.
(17) (a) Balch, A. L.; Catalano, V. J.; Noll, B. C.; Olmstead, M. M. *J. Am. Chem. Soc.* **1990**, *112*, 7558–7566. (b) Balch, A. L.; Catalano, V. J.; Olmstead, M. M. *J. Am. Chem. Soc.* **1990**, *112*, 2010–2011. (c) Balch, A. L.; Catalano, V. J. *Inorg. Chem.* **1991**, *30*, 1302–1308.

Table 10. Luminescent Spectral Data and Lifetime Measurements for the Compounds in the Solid State

compound	λ_{max} (298 K) emission [excitation]	λ_{max} (77 K) emission [excitation]	τ^a
[AuCl(PPh$_2$py)] (**1**)		499 [300]	
[AuCl(PPhpy$_2$)] (**3**)		499 [310]	
[Au$_2$CuCl$_2$(μ-PPh$_2$py)$_2$]BF$_4$ (**4**)	558 (+ sh) [320, 360]	552 (+ sh) [410]	29 μs
[Au$_2$CuCl$_2$(μ-PPh$_2$(CH$_2$)$_2$py$_2$)$_2$]PF$_6$ (**5**)	516 (br) [360]	520 (+ br) [370]	13 μs
[Au$_2$CuCl$_2$(μ-PPhpy$_2$)$_2$]BF$_4$ (**6**)	715 [460]	708 [465]	
[AuIrCl$_2$(μ-PPh$_2$py)(cod)] (**8**)		608 (+ sh) [470]	
[AuIrCl$_2$(μ-PPhpy$_2$)$_2$(cod)] (**12**)		620, 711 [405, 500]	

[a] At 298 K.

Table 11. Energy and Composition of More Intense Electronic Transitions of Complex [Au$_2$CuCl$_2$(PPh$_2$py)$_2$](BF$_4$) (**4**)

[Au$_2$CuCl$_2$(PPh$_2$py)$_2$](BF$_4$) (**4**)

excitation	composition	energy (eV)	wavelength (nm)	λ_{max}[a] (nm)	f ($\times 10^3$)
1	HOMO→LUMO (99%)	2.281	544		4.97
2	HOMO-1→LUMO (93%), HOMO→LUMO+1 (7%)	2.397	517	470−510	4.08
3	HOMO→LUMO+1 (92%), HOMO-1→LUMO (7%)	2.443	508		17.26
4	HOMO-3→LUMO+1 (80%) HOMO→LUMO+2 (12%), HOMO-5→LUMO (5%), HOMO→LUMO+3 (3%)	2.942	421		4.43
5	HOMO→LUMO+2 (85%), HOMO-3→LUMO+1 (11%)	2.956	420	405	5.80
6	HOMO-6→LUMO (72%), HOMO→LUMO+4 (13%)	3.21	386		33.37
7	HOMO-9→LUMO+1 (68%), HOMO-8→LUMO+1 (17%)	3.42	362		25.77
8	HOMO-13→LUMO+1 (36%), HOMO→LUMO+6 (16%), HOMO-5→LUMO+2 (12%), HOMO-6→LUMO+1 (11%)	3.58	347	320	1.34

[a] Experimental value (DRUV).

other hand, the same dσ* → pσ transitions have been proposed as the origin of the luminescence in other Au/Rh compounds,[18] but the Au/Rh complexes **7**, **9**, and **11** are nonemissive.

DFT Calculations. DFT calculations[19] (Amsterdam Density Functional (ADF) program)[20] were performed on the trinuclear complex **4** [Au$_2$CuCl$_2$(PPh$_2$py)$_2$](BF$_4$), and the two binuclear analogues [AuCl(PPh$_2$py)M(cod)-Cl] with M = Rh (**7**), Ir (**8**), to gain more knowledge about the luminescent behavior of these complexes.

The geometries of the three complexes were fully optimized without any symmetry constraints and considering all phenyl groups (see Computational Details), as they are usually needed to reproduce the luminescent behavior of complexes.[21]

A good agreement between experimental and calculated structural parameters is observed (tables with distances are given in the Supporting Information, Table S1). The most difficult distances to reproduce are those involving weak interactions, which in these complexes refer to the metal−metal distances. The Rh···Au distance in **7** was calculated as 3.068, and the experimental value is 3.0385 Å, while the Ir···Au distances in complex **8** are 3.111 (calculated) and 3.0148 Å (experimental). In the trinuclear **4**, the Au···Au distance is overestimated (3.279 vs 3.0658(5) Å), while the two calculated Au···Cu distances are shorter (2.794, 2.810 Å) than the experimental ones (2.9827(11), 3.0485(11) Å). The Mayer indices[22] are 0.244 (Rh···Au in **7**) and 0.212 (Ir···Au in **8**). Although these numbers are not directly comparable, they indicate a weak bond between Au and the second metal in both complexes. The geometry of the two binuclear complexes **7** and **8** was also optimized considering spin orbit coupling, but there was no change in the calculated M···Au distances.

TD-DFT calculations[23] were performed to interpret the electronic spectra of the three complexes. The most relevant results concerning the three complexes are collected in Tables 11−13, while the calculated spectra can be seen in Figure 9.

For the trinuclear [Au$_2$CuCl$_2$(PPh$_2$py)$_2$]BF$_4$ **4**, the observed maxima are found at 320, 405, and 470−510 nm. As shown in Figure 9, the calculated bands are all a bit shifted toward lower energies, with the most intense band between 350 and 450 nm, a shoulder at ∼420 nm, and other weaker absorptions in the range 480−550 nm. It should be noticed, in all the calculated spectra plotted in Figure 9, that the curves are obtained from a fit over several bands taking into account the respective oscillator strengths. This leads to observed maxima that may not coincide with the discrete values present in Tables 11−13. The calculated maximum at 372 nm has main contributions from two excitations at 386 and 362 nm, respectively, which start from the highest occupied molecular orbital (HOMO), HOMO-6, HOMO-8, and HOMO-9, and end mostly in lowest occupied molecular orbital (LUMO), and LUMO+1. The occupied orbitals are strongly localized in the copper atom (HOMO, 57%, and

(18) Yip, H. K.; Lin, H. M.; Wang, Y.; Che, C. M. *Inorg. Chem.* **1993**, *32*, 3402–3407.
(19) Parr, R. G.; Young, W. *Density Functional Theory of Atoms and Molecules*; Oxford University Press: New York, 1989.
(20) (a) *ADF2007*; SCM, Theoretical Chemistry, Vrije Universiteit: Amsterdam, The Netherlands; http://www.scm.com. (b) te Velde, G.; Bickelhaupt, F. M.; van Gisbergen, S. J. A.; Guerra, C. F.; Baerends, E. J.; Snijders, J. G.; Ziegler, T. *J. Comput. Chem.* **2001**, *22*, 931–967. (c) Guerra, C. F.; Snijders, J. G.; te Velde, G.; Baerends, E. J. *Theor. Chem. Acc.* **1998**, *99*, 391–403.
(21) Costa, P. J.; Calhorda, M. J. *Inorg. Chim. Acta* **2006**, *359*, 3617–3624.
(22) Mayer, I. *Int. J. Quantum Chem.* **1986**, *29*, 73–84.
(23) (a) van Gisbergen, S. J. A.; Snijders, J. G.; Baerends, E. J. *Comput. Phys. Commun.* **1999**, *118*, 119–138. (b) Rosa, A.; Baerends, E. J.; van Gisbergen, S. J. A.; van Lenthe, E.; Groeneveld, J. A.; Snijders, J. G. *J. Am. Chem. Soc.* **1999**, *121*, 10356–10365. (c) Wang, F.; Ziegler, T. *Mol. Phys.* **2004**, *102*, 2585–2595.

Table 12. Energy and Composition of More Intense Electronic Transitions of Complex [AuCl(PPh$_2$py)Rh(cod)Cl] (**7**)

[AuCl(PPh$_2$py)Rh(cod)Cl] (**7**)

excitation	composition	energy (eV)	wavelength (nm)	λ_{max}[a] (nm)	f ($\times 10^3$)
1	HOMO→LUMO+2 (96%), HOMO-1→LUMO (3%)	1.969	630		7.86
2	HOMO-1→LUMO (89%), HOMO→LUMO+3 (5%)	2.010	617		15.50
3	HOMO→LUMO+3 (88%), HOMO→LUMO+4 (5%), HOMO-1→LUMO+1 (4%)	2.240	554		21.32
4	HOMO→LUMO+4 (93%), HOMO→LUMO+3 (4%)	2.387	520		16.60
5	HOMO→LUMO+5 (95%), HOMO→LUMO+7 (3%)	2.629	472		8.14
6	HOMO→LUMO+6 (28%), HOMO-6→LUMO (20%), HOMO→LUMO+7 (18%), HOMO-7→LUMO (13%), HOMO-2→LUMO+3 (11%)	3.035	409	410−500	13.23
7	HOMO-6→LUMO (57%), HOMO→LUMO+7 (16%), HOMO→LUMO+6 (12%), HOMO-7→LUMO (8%)	3.043	407		13.44
8	HOMO-8→LUMO (45%), HOMO-7→LUMO (23%), HOMO-6→LUMO (12%)	3.260	380		56.42
9	HOMO-6→LUMO+1 (78%), HOMO-2→LUMO+5 (8%)	3.443	360		10.57
10	HOMO-6→LUMO+2 (62%), HOMO-10→LUMO (22%), HOMO-11→LUMO (8%)	3.655	339		8.40
11	HOMO-10→LUMO (34%), HOMO-11→LUMO (33%), HOMO-6→LUMO+2 (29%)	3.662	339		11.56
12	HOMO-11→LUMO (57%), HOMO-10→LUMO (36%)	3.694	336	325	18.86
13	HOMO-8→LUMO+2 (92%)	3.799	326		10.57
14	HOMO-2→LUMO+7 (73%), HOMO-9→LUMO+1 (5%), HOMO-3→LUMO+7 (4%)	3.850	322		10.33
15	HOMO-6→LUMO+4 (85%), HOMO-4→LUMO+6 (4%)	4.078	304		13.63

[a] Experimental value (DRUV).

Table 13. Energy and Composition of More Intense Electronic Transitions of Complex [AuCl(PPh$_2$py)Ir(cod)Cl] (**8**)

[AuCl(PPh$_2$py)Ir(cod)Cl] (**8**)

excitation	composition	energy (eV)	wavelength (nm)	λ_{max}[a] (nm)	f ($\times 10^3$)
1	HOMO-1→LUMO (76%), HOMO→LUMO+3 (12%), HOMO-1→LUMO+1 (8%)	2.0720	599		21.90
2	HOMO→LUMO+3 (74%), HOMO-1→LUMO+1 (12%), HOMO→LUMO+4 (6%), HOMO-1→LUMO (4%)	2.2454	552		23.40
3	HOMO-1→LUMO+1 (72%), HOMO→LUMO+4 (11%), HOMO-1→LUMO (9%)	2.3331	531		18.80
4	HOMO→LUMO+4 (81%), HOMO→LUMO+3 (7%), HOMO-1→LUMO+1 (4%)	2.3841	520		25.52
5	HOMO→LUMO+5 (93%), HOMO→LUMO+6 (5%)	2.613	474		7.09
6	HOMO-4→LUMO+1 (84%), HOMO→LUMO+6 (14%)	3.0261	410		11.63
7	HOMO→LUMO+6 (72%), HOMO-4→LUMO+1 (15%)	3.0580	405		41.40
8	HOMO-8→LUMO (59%), HOMO-1→LUMO+6 (15%)	3.3958	365		30.59
9	HOMO-6→LUMO+1 (86%), HOMO-8→LUMO (4%)	3.516	353	350	13.41
10	HOMO-9→LUMO (78%), HOMO→LUMO+7 (11%)	3.6147	343		14.38
11	HOMO-11→LUMO (27%), HOMO-10→LUMO (23%), HOMO-8→LUMO+1 (20%), HOMO→LUMO+8 (8%)	3.7600	330		28.17
12	HOMO-7→LUMO+2 (93%)	3.8923	318		13.49
13	HOMO-6→LUMO+4 (68%), HOMO-3→LUMO+6 (8%), HOMO→LUMO+10 (7%), HOMO-11→LUMO+1 (6%)	4.1416	299		11.88

[a] Experimental value (DRUV).

HOMO-6, 68%). The HOMO has a small contribution (8%) from each gold atom and is Au−Cu antibonding; HOMO-8 and HOMO-9 have some localization in copper and two phenyl groups of the phosphines, while the unoccupied orbitals (LUMO and LUMO+1) are concentrated on the pyridine rings (LUMO and LUMO+1). The transition can therefore be assigned as a charge transfer from Cu to the pyridine ligands (MLCT), with some mixture of ILCT (from the phenyl to the pyridine). The orbitals involved are shown in Figure 10 (the compositions of the orbitals of the three complexes are given in Supporting Information, Table S2). The three excitations contributing to the lower energy maximum (1, 2, and 3 in Table 11) start in HOMO and HOMO-1 and end in LUMO and LUMO+1. The HOMO-1 is strongly Au−Cl antibonding and Au−Cu antibonding, being delocalized between each metal (∼15%) and Cl (21 and 25%). This absorption can thus be assigned as MMLCT, involving orbitals localized on the Cu and Au d orbitals and Au−Cl orbitals to orbitals localized on the pyridyl rings. Therefore, excitation in these ranges involves not only IL states, but also MMCT (MMLCT becoming more important at low energies).

The calculated spectra of the binuclear Au−Rh (**7**) and Au−Ir (**8**) in the 300−400 nm range are different (Figure 9, Tables 12 and 13), since the Rh complex exhibits two maxima with comparable intensity at 326 and 383 nm, while in the Ir complex the maximum at 315 nm is much more intense than the one at 403 nm. These probably correspond to the maxima experimentally observed at 325 (**7**) and 350 nm (**8**). In the lower energy range (450−650), there are broad bands for both complexes.

Five transitions (11 to 15 in Table 12) are responsible for the peak at 326 nm (**7**). They start in HOMO-2, HOMO-6, HOMO-8, HOMO-10, and HOMO-11 and end in LUMO, LUMO+2, and LUMO+7, contributing in similar amounts to the higher energy band. The occupied orbitals have different compositions, namely, Rh−Cl (HOMO-2), Au−Cl and Rh−Cl (HOMO-6), Rh−Cl and COD (HOMO-8), Au−Cl, phenyl, and COD (HOMO-10),

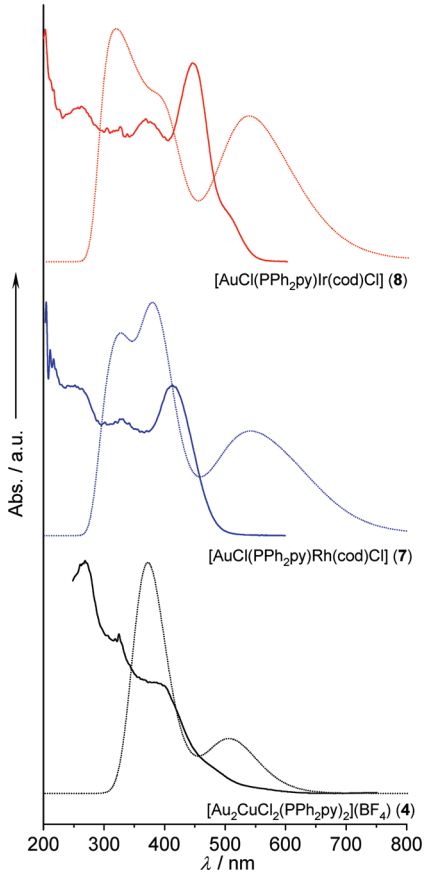

Figure 9. Calculated (TD-DFT; dotted line) and experimental (DRUV; solid line) spectra of complexes $[Au_2CuCl_2(PPh_2py)_2](BF_4)$ (**4**) and [AuCl(PPh2py)M(cod)Cl] with M = Rh (**7**), Ir (**8**).

and Au−Cl in HOMO-11. The LUMO is localized in the pyridine ring, LUMO+2 in the phenyl groups, and LUMO+7 on COD and Ph, with a small contribution of Rh. The main character of this band can be thus described as MLCT. The orbitals involved in these transitions are depicted in Figure 11. The peak at 383 nm consists of one intense transition (8 in Table 12) from HOMO-8, HOMO-7, and HOMO-6 to the LUMO. As HOMO-7 is similar to HOMO-6, this transition is a MMLCT from Au and Rh to the pyridine ring.

The band in the lower energy region results mainly from the transitions 2−4 (Table 12), and differs significantly from the others. These excitations start in the HOMO (71% Rh) and HOMO-1 (antibonding Rh−Cl; Rh 49%, Cl 41%), and end in LUMO (py ring), LUMO+3 and LUMO+4 (phenyl rings). Therefore, this band can be assigned essentially to a MLCT from Rh and Rh−Cl to the pyridine and phenyl rings.

For the Au−Ir complex (**8**), the higher energy band, calculated at 315 nm consists of several transitions. The most important ones are 10−12 (Table 13), starting in HOMO (Ir), HOMO-7 and HOMO-8 (Au, Ir−Cl, COD), HOMO-9 (Au, Ir−Cl, COD), HOMO-10 (Au−Cl, Ph, COD), and HOMO-11 (Au−Cl, Ir−Cl, COD), and ending in LUMO and LUMO+1 (pyridine), LUMO+2 (PPh_2), LUMO+7 (Ir−Cl, pyridine, COD), and LUMO+8 (Au, PPh_2). This transition has essentially MMLCT character (from Au and Ir to pyridine) with some mixed LLCT (Cl and COD to pyridine), in contrast to the corresponding

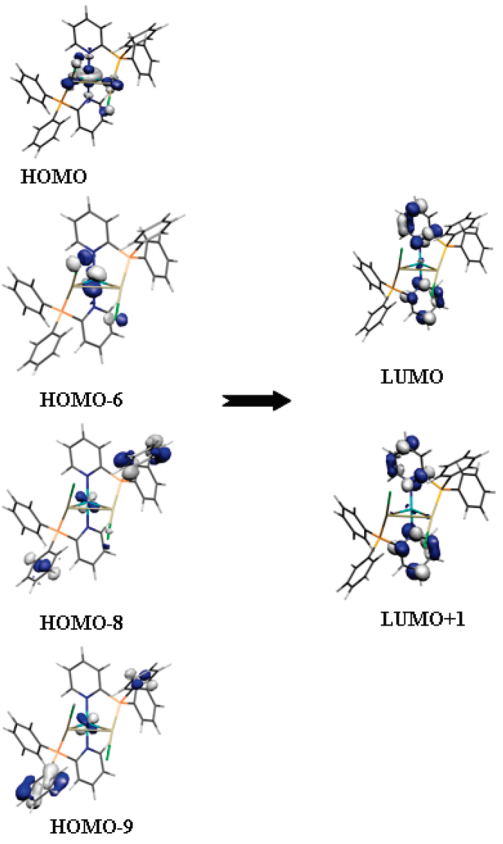

Figure 10. Relevant frontier orbitals of $[Au_2CuCl_2(PPh_2py)_2](BF_4)$ (**4**) involved in the transitions around 372 nm.

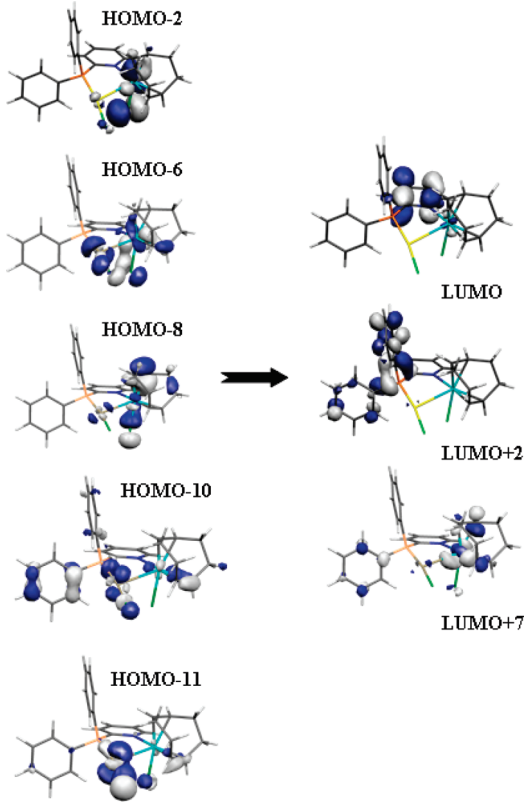

Figure 11. Relevant frontier orbitals of complex [AuCl(PPh2py)Rh-(cod)Cl] (**7**) involved in the transitions around 326 and 383 nm.

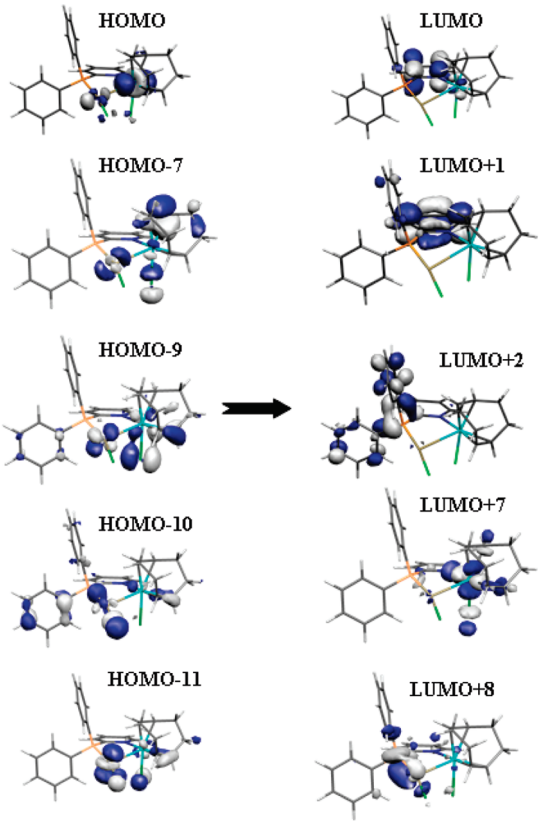

Figure 12. Relevant frontier orbitals of complex [AuCl(PPh$_2$py)Ir(cod)Cl] (**8**) involved in the transitions around 315 and 403 nm.

one in the Rh derivative **7**. A shoulder can be assigned to transition 8, from HOMO-8 (Ir−Cl, Au) and HOMO-1 (Ir−Cl) to LUMO (pyridine) and LUMO+6 (Ir-COD and Ph), and exhibits a MMLCT nature. The band calculated at 403 nm comes from transition 7 (Table 13) mostly (72%), starting in HOMO (Ir) and ending in LUMO+6 (Ir-COD and Ph), with MLCT character. The orbitals involved in these transitions are depicted in Figure 12. The lower energy band has contributions from excitations 1−4 (Table 13), starting in the HOMO and HOMO-1, and ending in LUMO, LUMO+1, LUMO+3, and LUMO+4. Both LUMO+3 and LUMO+4 are located in the phenyl rings. This transition can be assigned as MLCT.

The low energy bands of the Au−Ir (**8**) complex (transitions 1−7) have a significant participation of the HOMO and HOMO-1, which are orbitals heavily localized in Ir or Ir−Cl, while the comparable transitions in Au−Rh (**7**) have a negligible participation of HOMO and HOMO-1. Since the calculated excitation energy is at 500 and 450 nm, and these bands fall in the range of experimental excitation energy, the different emission behavior of the two complexes might be related to this. The higher energy orbitals that would contribute to higher energy excitations (~300−400 nm) are much more delocalized over the whole molecule in the Au−Ir (**8**) complex (see Figures 11 and 12).

The emission energy was estimated by the difference between the energy of the first triplet state and the energy of the singlet state with the same geometry. Therefore, the geometry of the first triplet state was optimized for the three molecules. The different electron−electron repulsion in the open shell excited states leads to some inversion in the order of orbitals with close energies in the ground state, with consequences in the nature of the frontier orbitals and the geometric details.

In complex **4**, the most visible change in geometry concerns the metal−metal bond lengths. The Cu−Au distances decrease as a result of removing one electron from the Cu−Au antibonding HOMO. The other bonds experience only slight changes (less than 0.05 Å). In the Au−Rh binuclear **7**, the Au−Rh bond decreases significantly from 3.068 in the ground state to 2.887 Å in the triplet state, and in **8** the Au−Ir bond shrinks from 3.111 to 2.895 Å, respectively.

The calculated emission energy for complex **4** is 509 nm, very close to the experimentally determined values in the range 520−558 nm. For the Au−Ir complex **8**, the calculated emission is 807 nm, a bit shifted from the experimental value (ca. 700 nm). Finally, for the Au−Rh complex **7**, an emission value of 921 nm could be calculated, although it was not observed experimentally.

The triplet state has a higher energy relative to the ground state in the Au−Ir derivative, where the metal−metal bond decreases by 0.220 Å, more than in the Au−Rh compound where the bond only shortens 0.178 Å. On the other hand, the nature of the highest singly occupied molecular orbital is different in the two complexes (SOMO in Figure 13). In the Au−Rh complex, the SOMO is a π bonding orbital between Rh and the pyridine ring, similar to the LUMO in the ground state (Figure 11), while in the Ir analogue it is almost completely localized in one π^* orbital of the phenyl rings (the ground state LUMO+2, Figure 12). The other singly occupied MO (SOMO-1 in Figure 13) is the M−Cl antibonding MO for both complexes (ground state HOMO-1). These two factors are probably associated with the emissive nature of the Au−Ir complex **8** and the non emissive nature of the Au−Rh complex **7**.

Conclusions

Several heterometallic complexes have been synthesized starting from the metalloligands [AuCl(P−N)], in which P−N represents a heterofunctional phosphine, by reaction with other metal centers. The structure of the complexes depends on the heterofunctional ligand and the heterometal. Thus the phosphines PPh$_2$py and PPhpy$_2$ favor the gold-heterometal interaction, whereas PPh$_2$CH$_2$CH$_2$py with a longer backbone precludes the metal−metal interaction. There are also differences between the first two phosphines, because PPh$_2$py has only one pyridine group available for bonding and PPhpy$_2$ has two and can afford tetra-coordination to the heterometal. These changes are key in the luminescence properties showed by these derivatives. The influence of the monophosphine, the presence or absence of a heterometal, and the selected heterometal in the emission energies led us to propose an origin for the observed emissions, which is supported by DFT theoretical studies carried out on some of the heterometallic complexes. The data and final assignments may be summarized as follows. (i) The metalloligands show weak luminescence only at low temperature, but the coordination of a heterometal generally enhances the luminescent properties. (ii) DFT calculations for the Au/Cu complex **4** suggest a MLCT origin (mostly MMLCT and mixed with some ILCT) for the observed emissions, which

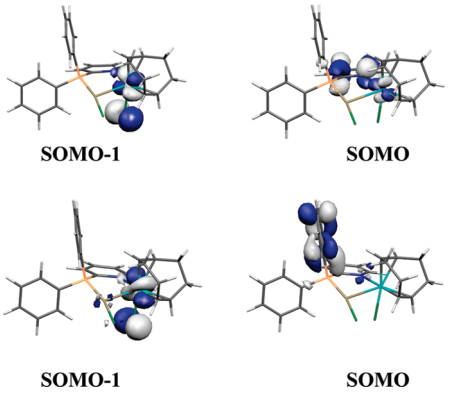

Figure 13. SOMOs in the triplet state of complexes [AuCl(PPh$_2$py)Rh(cod)Cl] (**7**, top) and [AuCl(PPh$_2$py)Ir(cod)Cl] (**8**, bottom).

partly supports the empirical proposal of an IL assignment based on the emission energy for **4** and **5**. The emission energy for compound **6** appears at much lower energy and is tentatively assigned as based in MLCT. (iii) The Au/Rh complexes are not emissive, and the luminescence in the Au/Ir derivatives seems to be determined by the different nature of the highest energy level in the triplet state leading to luminescence, which is localized in one phenyl ring in the Ir complex, but is a π bonding orbital between Rh and the pyridine ring in the other complex.

Experimental Section

Instrumentation. Infrared spectra were recorded in the range 4000−200 cm^{-1} on a Perkin-Elmer 883 spectrophotometer using Nujol mulls between polyethylene sheets. Conductivities were measured in about 5×10^{-4} mol dm^{-3} acetone solutions with a Philips 9509 conductimeter. C, H, N, and S analyses were carried out with a Perkin-Elmer 2400 microanalyzer. Mass spectra were recorded on a VG Autospec, with the liquid secondary-ion mass spectra (LSIMS) technique, using nitrobenzyl alcohol as matrix. NMR spectra were recorded on Bruker ARX 400 spectrometers in $CDCl_3$, unless otherwise stated. Chemical shifts are cited relative to $SiMe_4$ (^{1}H, external), $CFCl_3$ (^{19}F, external), and 85% H_3PO_4 (^{31}P, external). DRUV spectra were recorded with a UnicamUV-4 spectrophotometer equipped with a Spectralon RSA-UC-40 Labsphere integrating sphere. The solid samples were mixed with dried KBr and placed in a homemade cell equipped with a quartz window. The intensities were recorded in Kubelka−Munk units: $\log[R/(1-R)^2]$, where R = reflectance. Steady-state photoluminescence spectra were recorded with a Jobin-Yvon Horiba Fluorolog FL-3-11 spectrometer using band pathways of 3 nm for both excitation and emission. Phosphorescence lifetimes were recorded with a Fluoromax phosphorimeter accessory containing a UV xenon flash tube at a flash rate between 0.05 and 25 Hz. The lifetime data were fit using the Jobin-Yvon software package[24] and the Origin 5.0 program.[25]

Starting Materials. The starting materials PPh$_2$CH$_2$CH$_2$py,[26] PPhpy$_2$,[27] [Cu(NCMe)$_4$]PF$_6$,[28] [Rh(μ-Cl)(cod)]$_2$,[29] [Ir(μ-Cl)(cod)]$_2$,[30] [PdCl$_2$(NCPh)$_2$],[31] [AuCl(tht)][32] were prepared according to published procedures. All other reagents were commercially available.

Synthesis of [AuCl(P−N)] (P−N = PPh$_2$py (1), PPh$_2$CH$_2$CH$_2$py (2), PPhpy$_2$ (3)). To a solution of [AuCl(tht)] (0.032 g, 0.1 mmol) in 20 mL of dichloromethane was added PPh$_2$py (0.0263 g, 0.1 mmol) or PPh$_2$CH$_2$CH$_2$py (0.0291 g, 0.1 mmol) or PPhpy$_2$ (0.0262 g, 0.1 mmol), and the mixture was stirred for 20 min. The solvent was evaporated until approximately 2 mL, and the addition of diethyl ether gave white solids of **1** (0.048 g, 97%), or **2** (0.043 g, 82%), or **3** (0.047 g, 95%). Complex **2**: elemental analysis calcd. (%) for $C_{17}H_{18}AuClNP$ (MW = 524): C, 43.57; H, 3.46; N, 2.67, found: C, 43.58; H, 3.48; N, 2.69. NMR data: $^{31}P\{^1H\}$ ($CDCl_3$, δ) 29.52 (s, 1P, PPh$_2$CH$_2$CH$_2$py). ^{1}H ($CDCl_3$, δ), 8.48 (d, br, 1H, py, $^3J_{H-H} \sim 4.5$ Hz), 7.72−7.43 (m, 10H, Ph), 7.57 (td, 1H, py, $^3J_{H-H} = 7.6$ Hz, $^4J_{H-H} = 1.7$ Hz), 7.13 (m, 2H, py), 3.10 (m, 2H, CH_2), 2.98 (m, 2H, CH_2).

Synthesis of [Au$_2$CuCl$_2$(μ-P−N)$_2$]X, (P−N = PPh$_2$py, X = BF$_4$ (4); PPh$_2$CH$_2$CH$_2$py, X = PF$_6$ (5); PPhpy$_2$, X = BF$_4$ (6)). To a solution of [AuCl(PPh$_2$py)] (**1**) (0.099 g, 0.2 mmol), or [AuCl(PPh$_2$CH$_2$CH$_2$py)] (**2**) (0.104 g, 0.2 mmol) or [AuCl(PPhpy$_2$)] (**3**) (0.096 g, 0.2 mmol) in 20 mL of dichloromethane under argon atmosphere was added [Cu(NCMe)$_4$]X (0.1 mmol), and the mixture was stirred for 20 min. The solution was concentrated to about 5 mL, and addition of OEt$_2$ gave a yellow solid of **4** (0.093 g, 82%), a white solid of **5** (0.106 g, 85%), or an orange solid of **6** (0.096 g, 84%).

Complex **4**: elemental analysis calcd (%) for $C_{34}H_{28}Cl_2Au_2CuBF_4N_2P_2$ (MW = 1141.73): C, 35.76; H, 2.47; N, 2.45 (%); found: C, 35.74; H, 2.47; N, 2.41. NMR data: $^{31}P\{^1H\}$ ($CDCl_3$, δ), 34.05 (s, 2P, PPh$_2$py). ^{1}H ($CDCl_3$, δ), 8.53 (m, 2H, py), 7.84 (m, 2H, py), 7.60−7.49 (m, 20 + 2H, Ph+py), 7.36 (m, 2H, py).

Complex **5**: elemental analysis calcd (%) for $C_{38}H_{36}Cl_2Au_2CuF_6N_2P_3$ (MW = 1257.5): C, 36.33; H, 2.88; N, 2.23; found: C, 36.12; H, 2.30; N, 2.23. NMR data, $^{31}P\{^1H\}$ ($CD_3)_2CO$, δ), 29.42 (s, 2P, PPh$_2$CH$_2$CH$_2$py). ^{1}H (CD_2Cl_2, δ), 8.63 (m, 2H, py), 7.80 (m, 2H, py), 7.67−7.36 (m, 20 + 4H, Ph+py), 3.24 (m, 4H, CH_2), 3.04 (m, 4H, CH_2). Complex **6**: elemental analysis calcd (%) for $C_{32}H_{26}Cl_2Au_2CuBF_4N_4P_2$ (MW = 1143.71): C, 33.60; H, 2.29; N, 4.89 (%); found: C, 33.40; H, 2.12; N, 4.53. NMR data, $^{31}P\{^1H\}$ ($CD_3)_2CO$, δ), 23.06 (s, 2P, PPhpy$_2$). ^{1}H ($CD_3)_2CO$, δ), 8.56 (m, 4H, py), 8.20 (m, 8H, Ph), 7.98 (m, 4H, py), 7.86 (m, 2 + 4H, Ph+py), 7.73 (m, 4H, py).

Synthesis of [AuMCl$_2$(μ-PPh$_2$py)(cod)] (M = Rh (7), Ir (8)). To a solution of [AuCl(PPh$_2$py)] **1** (0.049 g, 0.1 mmol) in 20 mL of dichloromethane and under argon atmosphere was added [RhCl(cod)]$_2$ (0.024 g, 0.05 mmol) or [IrCl(cod)]$_2$ (0.033 g, 0.05 mmol), and the mixture was stirred for 20 min. The solvent was evaporated to about 5 mL, and the addition of diethyl ether gave a yellow solid of **7** (0.061 g, 83%) or the addition of hexane afforded an orange solid of **8** (0.059 g, 72%). Complex **7**: elemental analysis calcd (%) for $C_{25}H_{26}Cl_2AuNPRh$ (MW = 831.54): C, 40.45; H, 3.53; N, 1.89 (%); found: C, 40.30; H, 3.41; N, 1.82. NMR data, $^{31}P\{^1H\}$ ($CDCl_3$, δ), 32.59 (s, 1P, PPh$_2$py). ^{1}H ($CDCl_3$, δ), 8.79 (m, 1H, py), 7.99 (t, 1H, py, $^3J_{H-H} = 7.8$ Hz), 7.81 (tddd, 1H, *p*-Ph, $^3J_{H-H} = 7.7$ Hz, $^4J_{H-H} = 3.9$ Hz, $^4J_{H-H} = 1.8$ Hz), 7.72−7.37 (m, 9 + 2H, Ph+py), 4.22 (m, 4H, CH(cod)), 2.49 (m, 4H, CH_2(cod)), 1.74 (m, 4H, CH_2(cod)). Complex **8**: elemental analysis calcd (%) for $C_{25}H_{26}Cl_2AuIrNP$ (MW = 831.54): C, 36.10; H, 3.15; N, 1.68 (%); found: C, 35.95; H, 3.15; N, 1.56. NMR data, $^{31}P\{^1H\}$ ($CDCl_3$, δ), 32.35 (s, 1P, PPh$_2$py). ^{1}H ($CDCl_3$, δ), 8.62 (m, 1H, py), 8.05 (t, 1H, py, $^3J_{H-H} = 7.6$ Hz), 7.79 (m, 1H, Ph), 7.70−7.30 (m, 9 + 2H, Ph+py), 4.43 (m, 4H, CH(cod)), 2.91 (m, 4H, CH_2(cod)), 2.02 (m, 4H, CH_2(cod)).

Synthesis of [AuMCl$_2$(μ-PPh$_2$CH$_2$CH$_2$py)(cod)] (M = Rh (9), Ir (10)). To a solution of [AuCl(PPh$_2$CH$_2$CH$_2$py)] **2** (0.052 g,

(24) *DATAMAX*, 2.20; Jobin Yvon, Inc.: Edison, NJ, 2001.
(25) *Origin* 5.0; Microcal Software, Inc.: Northampton, MA, 1991.
(26) Casares, J. A.; Espinet, P.; Soulantica, K.; Pascual, I.; Orpen, A. G. *Inorg. Chem.* **1997**, *36*, 5251–5256.
(27) Xie, Y.; Chung, L. L.; Yang, Y.; Retting, S. J.; James, B. R. *Can. J. Chem.* **1992**, *70*, 751–762.
(28) Kubas, G. J. *Inorg. Synth.* **1979**, *19*, 90–92.
(29) Giordano, G.; Crabtree, R. H. *Inorg. Synth.* **1979**, *19*, 218–220.
(30) Herde, J. L.; Lambert, J. C.; Senoff, C. V. *Inorg. Synth.* **1974**, *15*, 18–20.
(31) Anderson, G. K.; Lin, M. *Inorg. Synth.* **1990**, *28*, 60–63.
(32) Usón, R.; Laguna, A.; Laguna, M. *Inorg. Synth.* **1989**, *26*, 85–91.

0.1 mmol) in 20 mL of dichloromethane was added $[RhCl(cod)]_2$ (0.024 g, 0.05 mmol) or $[IrCl(cod)]_2$ (0.033 g, 0.05 mmol), and the mixture was stirred for 20 min. The solution was concentrated to about 5 mL, and the addition of OEt_2 gave a yellow solid of **9** (0.065 g, 85%) or a yellow solid of **10** (0.079 g, 92%). Complex **9**: elemental analysis calcd (%) for $C_{54}H_{60}Cl_4Au_2N_2P_2Rh_2$ (MW = 1540.54): C, 42.10; H, 3.93; N, 1.82; found: C, 42.49; H, 3.53; N, 1.65. Λ_M (Ω^{-1} cm^2 mol^{-1}): 135. NMR data, $^{31}P\{^1H\}$ (CD_2Cl_2, δ), 32.41 (s, 1P, $PPh_2CH_2CH_2py$), 29.49 (s, 1P, $PPh_2CH_2CH_2py$). ^1H (CD_2Cl_2, δ), 8.79 (d, br, 1H, py, $^3J_{H-H} \sim$ 5.2 Hz), 8.47 (d, br, 1H, py', $^3J_{H-H} \sim$ 4.5 Hz), 8.06 (m, 2H, py+py'), 7.77−7.49 (m, 20H, Ph+Ph'), 7.34 (d, 1H, py, $^3J_{H-H}$ = 7.9 Hz), 7.20 (t, 1H, py, $^3J_{H-H}$ = 7.0 Hz), 7.10 (m, 2H, py+py'), 4.62−3.2 (m, 4 + 4H, CH(cod)+CH(cod)'), 2.95 (m, 8H CH_2CH_2), 2.39−1.25 (m, 8 + 8H, CH_2(cod)+CH_2(cod)'). Complex **10**: elemental analysis calcd (%) for $C_{54}H_{60}Cl_4Au_2Ir_2N_2P_2$ (MW = 1719.16): C, 37.72; H, 3.52; N, 1.63; found: C, 37.22; H, 3.20; N, 1.40. Λ_M (Ω^{-1} cm^2 mol^{-1}): 147. NMR data, $^{31}P\{^1H\}$ (CD_2Cl_2, δ), 32.38 (s, 1P, $PPh_2CH_2CH_2py$), 29.69 (s, 1P, $PPh_2CH_2CH_2py$). ^1H (CD_2Cl_2, δ), 8.66 (d, br, 1H, py, $^3J_{H-H} \sim$ 5.7 Hz), 8.47 (d, br, 1H, py', $^3J_{H-H} \sim$ 4.7 Hz), 7.99 (m, 2H, py+py'), 7.63−7.41 (m, 20 + 1H, Ph+Ph'+py), 7.28 (t, 1H, py', $^3J_{H-H}$ = 7.0 Hz), 7.13 (m, 2H, py), 4.43−3.10 (m, 4 + 4H, CH(cod)+CH(cod)'), 3.01 (m, 8H, CH_2CH_2), 2.59−1.25 (m, 8 + 8H, CH_2(cod)+CH_2(cod)').

Synthesis of [AuMCl$_2$(μ-PPhpy$_2$)(cod)] (M = Rh (11), Ir (12)). To a solution of [AuCl(PPhpy$_2$)] (**3**) (0.052 g, 0.1 mmol) in 20 mL of dichloromethane was added $[RhCl(cod)]_2$ (0.024 g, 0.05 mmol) or $[IrCl(cod)]_2$ (0.033 g, 0.05 mmol), and the mixture was stirred for 20 min. Then, the solvent was removed in vacuum to about 5 mL, and the addition of diethyl ether gave an orange solid of **11** (0.074 g, 77%) or a red solid of **12** (0.055 g, 67%). Complex **11**: elemental analysis calcd (%) for $C_{24}H_{25}Cl_2AuN_2PRh$ (MW = 743.21): C, 38.78; H, 3.39; N, 3.76; found: C, 38.52; H, 3.19; N, 3.50. NMR data, $^{31}P\{^1H\}$ (CD_2Cl_2, δ), 32.20 (s, 1P, $PPhpy_2$). ^1H (CD_2Cl_2, δ), 8.74 (d, br, 2H, py, $^3J_{H-H} \sim$ 4.6 Hz), 7.92 (dd, br, 2H, py, $^3J_{H-H} \sim$ 13.1 Hz, $^3J_{H-H} \sim$ 7.1 Hz), 7.84−7.55 (m, 5H, Ph), 7.50 (m, 2H, py), 7.39 (m, 2H, py), 4.22 (m, 4H, CH(cod)), 2.48 (m, 4H, CH_2 (cod)), 1.77 (m, 4H, CH_2 (cod)). Complex **12**: elemental analysis calcd (%) for $C_{24}H_{25}Cl_2AuIrN_2P$ (MW = 832.53): C, 34.62; H, 3.02; N, 3.36.; found: C, 34.30; H, 2.76; N, 3.02. NMR data, $^{31}P\{^1H\}$ (CD_2Cl_2, δ), 32.46. ^1H (CD_2Cl_2, δ), 9.21 (d, br, 1H, py, $^3J_{H-H} \sim$ 4.9 Hz), 8.75 (d, 1H, py, $^3J_{H-H} \sim$ 5.6 Hz), 7.97−7.41 (m, 5 + 6H, Ph+py), 3.66 (m, 4H, CH (cod)), 2.57 (m, 4H, CH_2 (cod)), 2.35 (m, 4H, CH_2 (cod)).

Synthesis of [Au$_2$PdCl$_4$(μ-P−N)$_2$] (P−N = PPh$_2$CH$_2$CH$_2$py (13), PPhpy$_2$ (14)). To a solution of [AuCl($PPh_2CH_2CH_2py$)] (**2**) (0.052 g, 0.2 mmol) or [AuCl($PPhpy_2$)] (**3**) (0.104 g, 0.2 mmol) in 20 mL of dichloromethane was added $[PdCl_2(NCPh)_2]$ (0.038 g, 0.1 mmol), and the mixture stirred for 20 min. The solution was concentrated to about 5 mL, and the addition of OEt_2 gave a yellow solid of **13** (0.105 g, 86%) or **14** (0.066 g, 57%). Complex **13**: elemental analysis calcd (%) for $C_{38}H_{36}Cl_4Au_2N_2P_2Pd$ (MW = 1224.81): C, 37.26; H, 2.96; N, 2.28; found: C, 37.45; H, 3.18; N, 2.42. NMR data, $^{31}P\{^1H\}$ ($CDCl_3$, δ), 29.90. ^1H ($CDCl_3$, δ), 8.86 (d, br, 2H, py, $^3J_{H-H} \sim$ 5.1 Hz), 7.81−7.15 (m, 20 + 6H, Ph+py), 4.20 (m, 4H, CH_2), 3.35 (m, 4H, CH_2). Complex **14**: elemental analysis calcd (%) for $C_{32}H_{26}Cl_4Au_2N_4P_2Pd$ (MW = 1170.68): C, 32.83; H, 2.23; N, 4.78; found: C, 32.40; H, 1.98; N, 4.32. NMR data, $^{31}P\{^1H\}$ (DMSO, δ), 30.19. ^1H (DMSO, δ), 9.17 (d, br, 4H, py, $^3J_{H-H} \sim$ 5.2 Hz), 8.24−7.59 (m, 10 + 8H, Ph+py), 7.33 (m, 4H, py).

Synthesis of [Au$_2$PtCl$_4$(μ-P−N)$_2$] (P−N = PPh$_2$py (15), PPh$_2$CH$_2$CH$_2$py (16), PPhpy$_2$ (17)). To a solution of [AuCl(PPh_2py)] (**1**) (0.099 g, 0.2 mmol), or [AuCl($PPh_2CH_2CH_2py$)] (**2**) (0.052 g, 0.2 mmol) or [AuCl($PPhpy_2$)] (**3**) (0.104 g, 0.2 mmol) in 20 mL of dichloromethane was added $[PtCl_2(NCPh)_2]$ (0.047 g, 0.1 mmol), and the mixture was stirred for 20 min. Then the solvent was evaporated to about 5 mL, and the addition of OEt_2 afforded yellow solids of **15** (0.098 g, 83%), or **16** (0.082 g, 67%) or **17** (0.090 g, 72%). Complex **15**: elemental analysis calcd (%) for $C_{34}H_{28}Cl_2Au_2N_2P_2Pt$ (MW = 1186.46): C, 34.42; H, 2.38; N, 2.36, found: C, 34.12; H, 2.17; N, 2.88. NMR data, $^{31}P\{^1H\}$ ($CDCl_3$, δ), 32.36 (s, 2P, PPh_2py). ^1H NMR ($CDCl_3$, ppm), 8.79 (d, br, 2H, py, $^3J_{H-H} \sim$ 4.7 Hz), 7.98 (t, 2H, py, $^3J_{H-H}$ = 7.8 Hz), 7.83−7.43 (m, 20 + 2H, Ph+py), 7.39 (m, 2H, py). Complex **16**: elemental analysis calcd (%) for $C_{38}H_{36}Cl_4Au_2N_2P_2Pt$ (MW = 1313.47): C, 34.75; H, 2.76; N, 2.13; found: C, 34.52; H, 2.41; N, 2.42. NMR data, $^{31}P\{^1H\}$ ($(CD_3)_2CO$, δ), 35.62 (s, 2P, $PPh_2CH_2CH_2py$). ^1H $(CD_3)_2CO$, δ), 8.50 (d, br, 2H, py, $^3J_{H-H} \sim$ 4 Hz), 8.05−7.57 (m, 20 + 2H, Ph+py), 7.40 (d, 2H, py, $^3J_{H-H}$ = 7.5 Hz), 7.28 (t, 2H, py, $^3J_{H-H}$ = 6.2 Hz), 3.26 (m, 4H, CH_2), 3.15 (m, 4H, CH_2). Complex **17**: Elemental analysis (%); Found: C, 31.12; H, 2.47; N, 4.04. Calculated for $C_{32}H_{26}Cl_4Au_2N_4P_2Pt$ (MW = 1259.34): C, 30.51; H, 2.08; N, 4.44. NMR data, $^{31}P\{^1H\}$ NMR ($(CD_3)_2CO$, ppm), 32.79 (s, 2P, $PPhpy_2$). ^1H NMR ($(CD_3)_2CO$, ppm), 8.78 (d, br, 4H, py, $^3J_{H-H} \sim$ 4.7 Hz), 8.04 (d, br, 4H, py, $^3J_{H-H} \sim$ 7.2 Hz), 8.07−7.90 y 7.67−7.55 (m, 10H, Ph), 7.85 (t, 4H, py, $^3J_{H-H} \sim$ 6.6 Hz), 7.75 (t, 4H, py, $^3J_{H-H} \sim$ 7.9 Hz).

Synthesis of [AuPdCl$_3$(μ-PPhpy$_2$)] (18). To a solution of [AuCl($PPhpy_2$)] (**3**) (0.052 g, 0.1 mmol) in 20 mL of dichloromethane was added $[PdCl_2(NCPh)_2]$ (0.047 g, 0.1 mmol), and the mixture was stirred for 20 min. Then the solvent was evaporated to about 5 mL, and the addition of OEt_2 afforded a yellow solid of **18** (0.047 g, 70%). Elemental analysis calculated for $C_{16}H_{13}Cl_3AuN_2PPd$ (MW = 674.006): C, 28.51; H, 1.94; N, 4.15; found: C, 28.19; H, 2.02; N, 3.99. NMR data, $^{31}P\{^1H\}$ ($CDCl_3$, δ), 30.34 (s, P, $PPhpy_2$). ^1H ($CDCl_3$, δ), 9.20 (m, 2H, py), 8.24 (m, 2H, py), 8.0 (m, 2H, py), 7.91−7.6 (m, 5H, Ph), 7.34 (m, 2H, py).

Crystallography. Crystals were mounted in inert oil on glass fibers and transferred to the cold gas stream of a Smart Apex CCD (**3**, **4**, **7**, **8**, **13**) or Xcalibur Oxford Diffraction (**9**, **12**, **18**) diffractometer equipped with a low-temperature attachment. Data were collected using monochromated Mo Kα radiation (λ = 0.71073 Å). Scan type ω. Absorption correction based on multiple scans were applied with the program SADABS.[33] The structures were refined on F^2 using the program SHELXL-97.[34] All non-hydrogen atoms were refined anisotropically. Hydrogen atoms were included using a riding model. Further details of the data collection and refinement are given in Tables 14 and 15.

Computational Details. All DFT calculations[19] were performed using the ADF program package (ADF).[20] Gradient corrected geometry optimizations,[35] without symmetry constraints, were performed using the Local Density Approximation of the correlation energy (Vosko−Wilk−Nusair),[36] and the Generalized Gradient Approximation (Perdew−Wang[37] exchange and correlation corrections). Relativistic effects were treated with the ZORA approximation.[38] Unrestricted calculations were performed for open shell species. The triplet state was obtained by promoting one electron from the HOMO to the LUMO. The core orbitals were frozen for Au, Ir ([1−4]s, [2−4]p, [3−4]d); Rh ([1−3]s, [2−3]p, 3d); Cu ([1−2]s, 2p); P, Cl ([1−2]s, 2p); and C and N (1s). Triple ζ Slater-type orbitals (STO) were used to describe the valence shells C, N (2s and 2p), P, Cl (3s, 3p), Au, and Ir (4f, 5d, 6s), Rh (4d, 5s), and Cu (3d, 4s). A set of two polarization functions was added to C, N (single ζ, 3d, 4f), P, Cl

(33) *SADABS*, Version 2.03; Bruker AXS, Inc: Madison, WI, 2000.
(34) Sheldrick, G. M. *SHELXL-97, A program for Crystal Structure Refinement*; University of Göttingen: Göttingen, Germany, 1997.
(35) (a) Versluis, L.; Ziegler, T. *J. Chem. Phys.* **1988**, *88*, 322–328. (b) Fan, L.; Ziegler, T. *J. Chem. Phys.* **1991**, *95*, 7401–7408.
(36) Vosko, S. H.; Wilk, L.; Nusair, M. *Can. J. Phys.* **1980**, *58*, 1200–1211.
(37) Perdew, J. P.; Chevary, J. A.; Vosko, S. H.; Jackson, K. A.; Pederson, M. R.; Singh, D. J.; Fiolhais, C. *Phys. Rev.* **1992**, *B46*, 6671–6678.
(38) van Lenthe, E.; Ehlers, A.; Baerends, E. J. *J. Chem. Phys.* **1999**, *110*, 8943–8953.

Table 14. X-ray Data for Complexes **3**, **4**, **7**, and **8**

	3	**4**	**7**	**8**
formula	$C_{16}H_{13}AuClN_2P$	$C_{36}H_{30}Au_2BCl_8CuF_4N_2P_2$	$C_{25}H_{26}AuCl_2NPRh$	$C_{25}H_{26}AuCl_2IrNP$
M_r	496.67	1380.44	742.21	831.50
habit	colorless prism	yellow plate	yellow prism	orange plate
crystal size (mm)	0.18 × 0.16 × 0.12	0.16 × 0.10 × 0.06	0.18 × 0.15 × 0.12	0.24 × 0.14 × 0.08
crystal system	monoclinic	monoclinic	monoclinic	monoclinic
space group	$P2_1/c$	$P2_1/c$	$P2_1/c$	$P2_1/c$
cell constants:				
a (Å)	7.9930(6)	13.1758(9)	13.630(3)	13.5661(15)
b (Å)	11.0534(8)	15.0406(10)	10.027(2)	10.0284(12)
c (Å)	17.7914(13)	22.4936(15)	18.563(4)	18.574(2)
β (deg)	99.0940(10)	101.6840(10)	103.98(3)	104.311(2)
V (Å^3)	1552.1(2)	4365.2(5)	2461.7(8)	2448.5(5)
Z	4	4	4	4
D_x (Mg m^{-3})	2.125	2.100	2.003	2.256
μ (mm^{-1})	9.747	7.799	6.919	11.712
$F(000)$	936	2616	1424	1552
T (°C)	−173	−173	−173	−173
$2\theta_{max}$	56.6	56	56	56.6
no. of refl.:				
measured	18572	25547	18623	15862
independent	3777	8596	4824	5803
transmissions	0.2729−0.3876	0.368−0.652	0.3113−0.4234	0.1654−0.4543
R_{int}	0.028	0.0422	0.0876	0.0432
parameters	190	505	280	280
restraints	0	27	0	0
$wR(F^2$, all Refl.)	0.0591	0.1028	0.1049	0.0855
$R(I, >2\sigma(I))$	0.0234	0.0461	0.0468	0.0366
max. $\Delta\rho$ (e Å^{-3})	1.914	3.263	1.011	1.026

Table 15. X-ray Data for Complexes **9**, **12**, **13**, and **18**

	9·H_2O	**12**·$1/2CH_2Cl_2$	**13**	**18**
formula	$C_{27}H_{32}AuCl_2NOPRh$	$C_{24.5}H_{25.5}AuCl_3IrN_2P$	$C_{43}H_{48}Au_2Cl_6N_2OP_2Pd$	$C_{20}H_{19}AuCl_3N_4PPd$
M_r	788.28	870.46	1383.81	756.08
habit	yellow prism	yellow plate	paleyellow prism	yellow plate
crystal size (mm)	0.22 × 0.20 × 0.12	0.24 × 0.22 × 0.08	0.25 × 0.20 × 0.18	0.20 × 0.10 × 0.08
crystal system	triclinic	monoclinic	monoclinic	monoclinic
space group	$P\bar{1}$	$P2_1/c$	$C2/c$	$C2/c$
cell constants:				
a (Å)	9.2224(18)	18.090(4)	22.3635(12)	21.195(4)
b (Å)	10.251(2)	17.031(3)	8.9788(5)	12.250(3)
c (Å)	15.128(3)	17.584(4)	24.3721(13)	18.531(4)
α (deg)	101.71(3)			
β (deg)	90.65(3)	114.23(3)	97.9210(10)	96.50(3)
γ (deg)	108.63(3)			
Z	2	8	4	8
D_x (Mg m^{-3})	1.979	2.351	1.896	2.101
μ (mm^{-1})	6.448	11.721	6.837	7.301
$F(000)$	764	3268	2656	2864
T (°C)	−173	−173	−173	−173
$2\theta_{max}$	51	50	57	51
no. of refl.:				
measured	8583	56190	15643	34557
independent	4772	8624	5722	4427
transmissions	0.3312−0.5117	0.165−0.454	0.279−0.372	0.323−0.592
R_{int}	0.0126	0.083	0.021	0.024
parameters	307	586	265	272
restraints	0	0	0	0
$wR(F^2$, all Refl.)	0.066	0.139	0.073	0.037
$R(I, >2\sigma(I))$	0.027	0.051	0.0279	0.017
S	1.066	1.059	1.038	1.141
max. $\Delta\rho$ (e Å^{-3})	1.29	2.88	2.24	0.95

(single ζ, 3d, 4p), Au, and Ir (single ζ, 6p, 5f), Rh (single ζ, 5p, 4f), and Cu (single ζ, 4p, 4f). Triple ζ Slater-type orbitals (STO) were used to describe the valence shells of H (1s) with two polarization functions (single ζ, 2s, 2p). Time dependent DFT calculations (TD-DFT)[23] in the ADF implementation were used to determine the excitation energies. The seventy lowest singlet−singlet excitation energies were calculated for the three complexes, using the optimized geometries. Mayer bond orders[22] and spin orbit coupling were calculated as implemented in ADF. Three-dimensional representations of the orbitals were obtained with Molekel,[39] and structures and electronic spectra with Chemcraft.[40]

Acknowledgment. We thank the Dirección General de Investigación Científica y Técnica (CTQ2007-67273-C02-01) for financial

(39) Portmann, S.; Lüthi, H. P. *Chimia* **2000**, *54*, 766–770.
(40) http://www.chemcraftprog.com/index.html.

support. M.J.C. and P.D.V. acknowledge FCT, POCI, and FEDER (project PTDC/QUI/58925/2004) for financial support.

Supporting Information Available: Eight X-ray crystallographic files, in CIF format, for compounds **3**, **4**, **7**, **8**, **9**, **12**, **13**, **18** (CCDC reference numbers 730877−730884). Tables S1 and S2, with results from DFT calculations (calculated distances and composition of frontier orbitals). This material is available free of charge via the Internet at http://pubs.acs.org.